Development of hemp nanocellulose-based plastic films for food packaging

Ziyu Liao

Department of Food Science and Agricultural Chemistry
Faculty of Agricultural and Environmental Sciences
McGill University, Montreal

September 2022

A thesis submitted to McGill University in partial fulfilment of the requirements of the degree of Master of Science

ABSTRACT

Most plastic food packaging is non-biodegradable and thus poses a serious threat to the environment. To address this problem, bioplastics have been developed as a green alternative to the conventional plastics because they are made from biodegradable polymers. Hemp stalk is a green waste that owns a high cellulose content and can be further processed to produce a value-added product known as nanocellulose. Nanocellulose can be utilized as a biodegradable material for use in bioplastics to improve their mechanical and barrier properties. In this thesis project, hemp stalk was separated into hemp bast fibers and hurd and used for cellulose extraction. Hemp hurd cellulose was obtained with a purity of 85% and a yield of 23.9%, while bast cellulose had a purity of 97% and a yield of 49.6%. Next, hemp bast cellulose was used as the raw material to prepare nanocellulose. Hemp cellulose nanocrystals (CNCs) were prepared via sulphuric acid hydrolysis and owned an average diameter of 16 nm and an average length of 244 nm. Hemp cellulose nanofibrils (CNFs) were synthesized by 2,2,6,6-tetramethylpiperidine-1-oxyl (TEMPO)-mediated oxidation with the addition of 8 mmol of sodium hypochlorite (NaClO)/g cellulose and displayed an average diameter of 24 nm and an average length of 292 nm. Both CNCs and CNFs showed a good compatibility in the Poly(vinyl alcohol) (PVA) film, and the addition of 10% nanocellulose significantly improved the strength, stiffness, and ultraviolet-blocking effect of PVA film. In addition, hemp CNFs, Poly-L-lysine hydrochloride (PLH), and PVA were used to develop a novel composite film. The film owned a high transparency, good mechanical performance, UV-blocking effect, and antimicrobial activities against several bacteria, including *Salmonella enterica* serotype Typhimurium, *Staphylococcus aureus*, *Escherichia coli*, and *Pseudomonas aeruginosa*. The PVA/CNF/PLH film has great potential to be applied as antimicrobial food packaging. The outcomes of this thesis project will promote the circular economy of the hemp industry by converting hemp

waste into value-added products and boost the sustainability of the food industry by providing an eco-friendly packaging solution.

RÉSUMÉ

La plupart des emballages alimentaires en plastique ne sont pas biodégradables et constituent donc une menace sérieuse pour l'environnement. Pour résoudre ce problème, les bioplastiques ont été développés comme une alternative verte aux plastiques conventionnels car ils sont fabriqués à partir de polymères biodégradables. La tige de chanvre est un déchet vert qui possède une forte teneur en cellulose et peut être traitée pour produire un produit à valeur ajoutée connu sous le nom de nanocellulose. La nanocellulose peut être utilisée comme matériau biodégradable dans les bioplastiques afin d'améliorer leurs propriétés mécaniques et de barrière. Dans ce projet de thèse, la tige de chanvre a été séparée en fibres libériennes et en chènevottes et utilisée pour l'extraction de la cellulose. La cellulose de la chènevotte a été obtenue avec une pureté de 85% et un rendement de 23,9%, tandis que la cellulose des fibres libériennes avait une pureté de 97% et un rendement de 49,6%. Ensuite, la cellulose grasse de chanvre a été utilisée comme matière première pour préparer la nanocellulose. Les nanocristaux de cellulose de chanvre (CNC) ont été préparés par hydrolyse à l'acide sulfurique et possédaient un diamètre moyen de 16 nm et une longueur moyenne de 244 nm. Les nanofibrilles de cellulose de chanvre (CNF) ont été synthétisées par oxydation médiée par le 2,2,6,6-tétraméthylpipéridine-1-oxyle (TEMPO) avec l'ajout de 8 mmol d'hypochlorite de sodium (NaClO)/g de cellulose et présentaient un diamètre moyen de 24 nm et une longueur moyenne de 292 nm. Les CNC et les CNF ont montré une bonne compatibilité dans le film de Poly(alcool vinylique) (PVA), et l'ajout de 10% de nanocellulose a amélioré de manière significative la résistance, la rigidité et l'effet de blocage des ultraviolets du film PVA. En outre, les CNF de chanvre, le chlorhydrate de poly-L-lysine (PLH) et le PVA ont été utilisés pour développer un nouveau film composite. Le film possède une grande transparence, une bonne performance mécanique, un effet de blocage des UV et des activités antimicrobiennes contre plusieurs bactéries, y compris *Salmonella enterica* sérotype Typhimurium, *Staphylococcus*

aureus, *Escherichia coli* et *Pseudomonas aeruginosa*. Le film PVA/CNF/PLH a un grand potentiel pour être appliqué comme emballage alimentaire antimicrobien. Les résultats de ce projet de thèse vont promouvoir l'économie circulaire de l'industrie du chanvre en convertissant les déchets de chanvre en produits à valeur ajoutée et stimuler la durabilité de l'industrie alimentaire en fournissant une solution d'emballage écologique.

ACKNOWLEDGMENT

I would like to express my sincere appreciation to my supervisor Dr. Xiaonan Lu for offering me this wonderful opportunity to join in his lab and providing me invaluable guidance and support throughout my master's study. The encouragement, recognition, and trust you gave really inspired me and promoted my efforts during this project and would be meaningful for my entire life. I am highly grateful to Dr. Yixiang Wang and Dr. Xin Zhao for serving as my supervisory committee members and kindly providing help on my thesis project.

My special thanks of gratitude also give to Dr. Zhilong Yu as my mentor that always elaborately taught and trained me skills not only in all the stages of this project, but also helped me in many other aspects. I am grateful for your efforts and time spent on directing me properly run and accomplish this project.

I would like to acknowledge the financial support from the funding agency, including the Investment Agriculture Foundation of British Columbia (IAFBC) and Canada-British Columbia Agri-innovation Program (CBCAIP).

My thanks and appreciations also go to Dr. Lixue Liu, Dr. Shaolong Feng, Bingxue Hu for teaching me basic experimental and machine operation skills and offering advises on experimental designs and data analysis. I am deeply indebted to all members in the Lu Lab for their support and all the treasure time we shared.

Lastly, I would like to thank my beloved parents and friends for their unconditional love, help, support, and encouragement that heal me during the challenging times. The accomplishment for the journey of this graduate study would not be possible without them.

PREFACE

This thesis was prepared by following the McGill University Thesis Preparation guidelines for graduate and postdoctoral studies. This thesis is expressed in traditional monograph-writing style, consists of five chapters: Introduction, Literature Review, Materials and Methods, Results and Discussion, and Conclusion. This work is original and has not been published previously.

CONTRIBUTION OF AUTHORS

Ziyu Liao is the primary author who is responsible for the five chapters of this thesis. Dr. Xiaonan Lu proposed this thesis project, and Dr. Zhilong Yu had direct advisory on the entire experimental scheme. Ziyu Liao conducted all the experiments, including hemp cellulose extraction, nanocellulose synthesis, and preparation and characterization of composite plastic films, and analyzed all the data. The staff scientist David Liu performed TEM and SEM testing for the hemp nanocellulose and packaging film samples in this project. This thesis was edited and guided by Dr. Lu and Dr. Yu.

TABLE OF CONTENTS

LIST OF FIGURES

LIST OF TABLES

LIST OF ABBREVIATIONS

AgNPs	Silver nanoparticles
APDMH	3-(3′- acrylicacidpropylester)-5,5-dimethylhydantoin
ATP	Adenosine triphosphate
ATR-FTIR	Attenuated Total Reflectance-Fourier Transform Infra-Red
AuNPs	Gold nanoparticles
BNC	Bacterial nanocellulose
CBD	Cannabidiol
CFU	Colony forming units
CNCs	Cellulose nanocrystals
CNFs	Cellulose nanofribrils
CuONPs	Copper oxide nanoparticles
EO	Essential oils
FDA	Food and Drug Administration
FTIR	Fourier transformed infrared
Gly	Glycerol
GRAS	Generally Recognized As Safe
H_2SO_4	Sulphuric acid
HCl	Hydrochloric acid
MAP	Modified atmosphere packaging
MRSA	Methicillin-resistant *Staphylococcus aureus*
NaClO	Sodium hypochlorite
$NaClO_2$	Sodium chlorite
$NaHSO_4$	Sodium bisulfate
NaOH	Sodium hydroxide

NC	Nanocellulose
PLA	Poly(lactic acid)
PLH	Poly-L-lysine hydrochloride
PVA	Poly(vinyl alcohol)
QAC	Quaternary ammonium compounds
ROS	Reactive oxygen species
SD	Standard deviation
SEM	Scanning Electron Microscopy
TAPPI	Technical Association of the Pulp and Paper Industry
TEM	Transmission Electron Microscopy
TEMPO	2,2,6,6-tetramethylpiperidine-1-oxyl
THC	Tetrahydrocannabinol
ZnONPs	Zinc oxide nanoparticles
ε-PL	Epsilon-poly-L-lysine

CHAPTER 1. INTRODUCTION

1.1 General Introduction

Hemp (*Cannabis sativa* subspecies L.) is a plant that has been cultivated for centuries and applied in various sectors, such as food, material, and medicine industries. A hemp plant is comprised of five main parts, including seeds, leaves, inflorescences, stalks, and roots. Hemp seeds are traditionally used to produce food products (*e.g.*, edible oil and protein flour), while hemp leaves and inflorescences are used for the extraction of cannabinoids and essential oil (Karche and Singh, 2019). However, the hemp stalks and roots are produced as wastes in the hemp industry and normally end up in landfill. There is a critical need to convert these green wastes into value-added products. Hemp stalk is composed of two main parts, including bast fibers in the outer layer and hurd in the inner part. Both of them are rich in cellulose and can be used to prepare nanocellulose (Stevulova et al., 2014; USDA, 2019). Nanocellulose is the cellulosic material with a structure at the nanometer scale. There are three main types of nanocellulose, including cellulose nanocrystals (CNCs), cellulose nanofibrils (CNFs), and bacterial nanocellulose (BNC). CNCs are synthesized through acid hydrolysis with the degradation of amorphous regions in cellulose fibers, and have a highly crystalline structure. CNFs are highly fibrillated cellulosic materials that are often produced using chemical, enzymatic, and mechanical methods (Arrieta et al., 2016; Tian et al., 2016; Du et al., 2019). BNC is a natural cellulose nanofiber produced by bacteria (Stanislawska, 2019). Nanocellulose has the advantages of being lightweight, biodegradable, and renewable. Additionally, nanocellulose has great potential to be used as a filler in food packaging to improve mechanical and barrier properties (Moon et al., 2010; Blanco et al., 2018).

Food packaging has been traditionally used for food preservation. Most plastic food packaging is made of non-biodegradable materials and designed for single use. In Canada, only 20% of food packaging wastes are recovered for recycling and reused, while the remaining

packaging wastes mainly end up in landfill that pose a threat to the environment (Tiseo, 2018; Brennan et al., 2020; Walker et al., 2021). To address this problem, researchers have paid considerable attention to developing bioplastics as alternatives to the conventional plastics. Since bioplastics are made from biodegradable synthetic polymers or biopolymers, they are sustainable and eco-friendly. However, the mechanical and barrier properties of bioplastics remain to be improved (Salgado et al., 2021). In addition, conventional food packaging are inert materials that cannot inhibit the growth of foodborne pathogens and spoilage bacteria. Thus, antimicrobial food packaging has been developed to improve food safety and quality (Yildirim, 2011). Polylysine is an antimicrobial biopolymer with the advantages of being non-toxic, biodegradable, water-soluble, and thermally stable. It is a generally recognized as safe (GRAS) material that has great potential for developing antimicrobial materials (You et al., 2017; Rodrigues et al., 2020). However, studies on the antimicrobial modification of food packaging by polylysine are rarely reported yet.

Recently, the application of hemp nanocellulose as the raw material for preparing biodegradable food packaging has seldom been reported. Moreover, the development of composite packaging film that consist of nanocellulose, bioplastics and polylysine has not been studied yet. Therefore, this project will investigate a novel work about the production of hemp nanocellulose-based antimicrobial bioplastic food packaging which would has great potential to be introduced as a new value-added and environmental-friendly packaging type to the food industry.

1.2 Research Hypotheses and Objectives

In this thesis project, there are three main hypotheses: (1) Cellulose in hemp stalk can be extracted and used for the synthesis of CNCs and CNFs. (2) Hemp nanocellulose can be incorporated in biodegradable packaging materials to develop novel composite films with

desirable mechanical and barrier properties. (3) Hemp nanocellulose and polylysine can be incorporated in biodegradable packaging materials to develop antimicrobial food packaging with potential for commercialization.

To test the proposed hypotheses, three main objectives should be accomplished: (1) utilizing hemp stalk as the raw material to extract nanocellulose, (2) developing novel bioplastic packaging incorporated with hemp nanocellulose, and (3) synthesizing antimicrobial bioplastic packaging incorporated with hemp nanocellulose and polylysine.

CHAPTER 2. LITERATURE REVIEW

2.1 Hemp

Hemp (*Cannabis sativa* subspecies L.) is a plant of the family *Cannabaceae* and has been utilized for centuries as the sources of oilseeds, herbal medicines, and fibers for rope, sailing canvas, and paper (Karche and Singh, 2019; Farinon et al., 2020). This plant was permitted for cultivation in Canada since 1998 and is currently regulated by Health Canada under the Cannabis Act. Canada is currently a leading hemp-producing country with 77,800 acres of hemp cultivated in 2018 (USDA, 2019). A typical hemp plant consists of stalks, seeds, leaves, inflorescences, and roots. The applications of hemp are shown in **Figure 2.1** and described in details in this section.

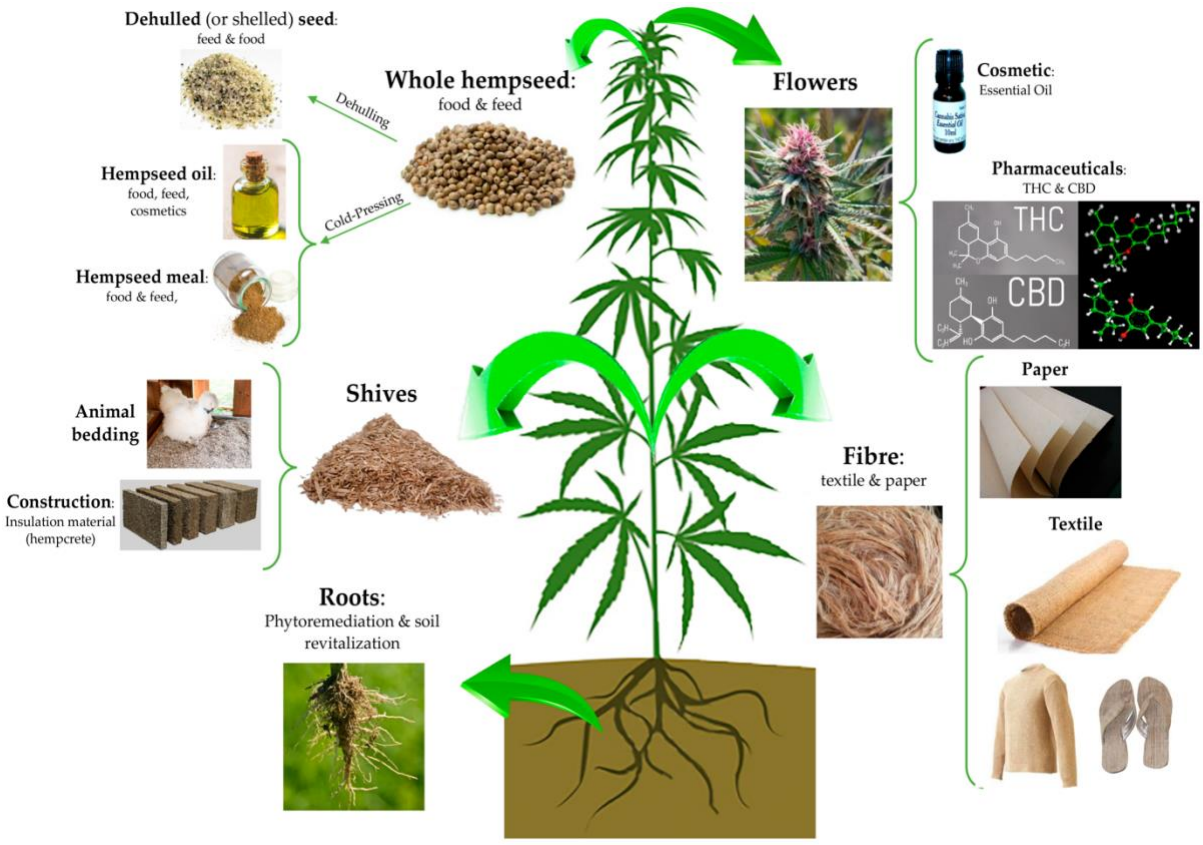

Figure 2.1 Applications of different parts of hemp plants in different industrial fields (Farinon et al., 2020).

2.1.1 Hemp seeds

Hemp seeds contain around 25%-30% lipids, 25%-30% proteins, and 30%-40% dietary fibers (Leonard et al., 2019). They also serve as a good source of vitamin E, vitamin B, and minerals such as calcium, iron, and phosphorous. Hemp seed oils have been used for the production of edible oils (Karche and Singh, 2019; Leonard et al., 2019). Over 80% of hemp seed oils are polyunsaturated fatty acids that are known for many health benefits. For example, omega-3 fatty acids (*e.g.*, α-linoleic acid) can support mental and heart health as well as reduce liver fat, while omega-6 fatty acids (*e.g.*, linoleic acid) are capable of providing required energy to human body and reduce the risks of chronic diseases and cancers. The optimal ratio of omega-6 to omega-3 fatty acids in hemp seed oil for promoting human health has been determined to be 3:1. Besides, hemp seed oils comprise other nutritional components, such as γ-linolenic acid, β-sitosterol, β-amyrin, and methyl salicylate. It is worth of mentioning that hemp seed oil is a potential renewable energy source since it can be converted into the biodiesel with low-emission properties (Karche and Singh, 2019).

After oil extraction, hemp seed cake owns a high content of proteins (>25%). There are two major proteins in the hemp seed cake, including legumin-type globulin edestin and globular-type albumin. Edestin has a high digestibility and can act as globulins in blood plasma to promote human immune systems (Leonard et al., 2019; Karche and Singh, 2019). In addition, hemp seed cake is rich in fibers (>30%). Particularly, the insoluble fibers are comprised of 46% cellulose, 31% lignin, and 22% hemicellulose. They can enhance fecal bulking and retard absorption of macronutrients, thereby capable of supporting bowel health and lowering the risk of diabetes and cancers. Thus, hemp seed cake has been utilized as a raw material to manufacture hemp protein powder with a high fiber level (Leonard et al., 2019; Karche and Singh, 2019).

2.1.2 Hemp leaves and inflorescences

Hemp leaves and inflorescences are raw materials for the extraction of cannabinoids and the production of essential oil. Cannabinoids are naturally occurring compounds found in cannabis. Major cannabinoids in hemp leaves and flowers comprise tetrahydrocannabinol (THC), cannabidiol (CBD), and terpenoids (*e.g.*, β-caryophyllene and limonene). Among them, CBD and THC are the most abundant types and have drawn considerable attention. Currently, the applications of CBD are more focused on medical treatments due to its remarkable biological activities, such as antiepileptic, antinociceptive, and anti-inflammatory activities. In addition, there are rising interests on developing novel CBD-infused foods and beverages for the use as functional foods to relieve pain and support the treatment of depression and anxiety. CBD oil that meets the THC limit (<0.3% on dry weight basis) required by the regulatory agency has been approved for sale and consumption (Charrette et al., 2021; VanDolah et al., 2019). Legal marketing of CBD-containing food products is being actively considered until enough data are collected to support the safe use of CBD oil (Charrette et al., 2021). THC is the main psychoactive component in cannabis that has great potential for medical use because it possesses mind-altering effects, intoxicating property, and appetite-stimulating properties especially for patients with cancer and acquired immune-deficiency syndrome (Karche and Singh, 2019).

Hemp essential oil is often extracted from the upper part of hemp leaves and flowers by steam distillation. The essential oil shows a pale yellowish color, and its main volatile compounds include monoterpenes and sesquiterpenes (Karche and Singh, 2019). The terpenes in hemp essential oil are lipophilic compounds owning multiple health benefits since they can easily penetrate through blood-brain barrier to display anti-inflammatory, analgesic, and anxiolytic activities. So far, hemp essential oil has been used as flavoring agents in food products such as beverages and bakery products, or added in cosmetics, soaps, and perfume to

impart an appealing scent (Vuerich et al., 2019). THC content in hemp essential oil is regulated in the range of 0.02%-0.08% (*w/w*). Besides, limonene and α-pinene, two volatile compounds in hemp essential oil, can be utilized as insecticides in agriculture (Mediavilla and Steinemann, 1997).

2.1.3 Hemp stalks

In the hemp industry, hemp stalks and roots are green wastes that often end up in landfill or go to the disposal system for deduction. Hemp stalks have limited applications for use as animal bedding materials and raw materials for fiber products such as paper and ropes. Noticeably, hemp stalks are difficult to be processed mechanically. The outer fiber shell of hemp stalk called bast is so tough that traditional machines used in conventional farming show low efficiency to break down the stalks. In addition, mechanical processing of hemp stalk (*e.g.*, decorticating and cutting) is time- and energy-consuming (Khan et al., 2010). Canada is one of the world-leading producers of hemp crops, with 77,800 acres of hemp cultivated in 2018. Every acre of hemp harvested produces approximately 2-5 tons of stalk waste annually (USDA, 2019). This large waste stream facilitates the demands for developing value-added products based on hemp stalk. Hemp stalk is composed of two parts: bast (20%-40%) and hurd (60%-80%). Bast is the long, tough fiber on the outer layer of hemp stalk that contains 57%-77% cellulose, 5%-9% lignin, and 9%-14% hemicellulose. Hurd is the short, soft fiber located in the inner part of hemp stalk that comprises 40%-48% cellulose, 21%-24% lignin, and 18%-24% hemicellulose (Stevulova et al., 2014). Because hemp stalk is rich in cellulose fibers, it can be utilized as a raw material for cellulose extraction.

2.2 Cellulose and cellulosic nanomaterials

2.2.1 Cellulose

Cellulose is the most abundant biomass and natural biopolymer on earth. It has been gaining increasing attention due to its renewability, biodegradability, and remarkable physical and mechanical properties (Tavakolian et al., 2020). As shown in **Figure 2.2**, cellulose is a linear polysaccharide consisted of repeating anhydro-D-glucopyranose units joint by β-1,4-glucosidic linkages and has a basic chemical formula of $(C_6H_{10}O_5)_n$. Cellulose chains are hierarchically combined together to produce microfibrils. This process involves the formation of van der Waals forces as well as intermolecular and intramolecular hydrogen bonds among molecular chains. Every cellulose microfibril is constituted of repeating well-ordered (crystalline) and disordered (amorphous) regions. Bundles of cellulose microfibrils are assembled into aggregates (macrofibrils) with combination of lignin and hemicellulose (Arrieta et al., 2016; Islam et al., 2018; Seddiqi et al., 2021). In nature, cellulose fibers function as an important structural element to support plant cell walls and are present in the tissues of algae and the cell membranes of tunicates (Seddiqi et al., 2021). Cellulose and its derivatives have been applied in various fields to produce diverse products, such as paper, tensile products, packaging, food additives, and biomedical materials for drug delivery and wound dressing. They can also be disintegrated into a nanoscale to prepare cellulosic nanomaterials with superior mechanical and surface properties (Dufresne, 2019).

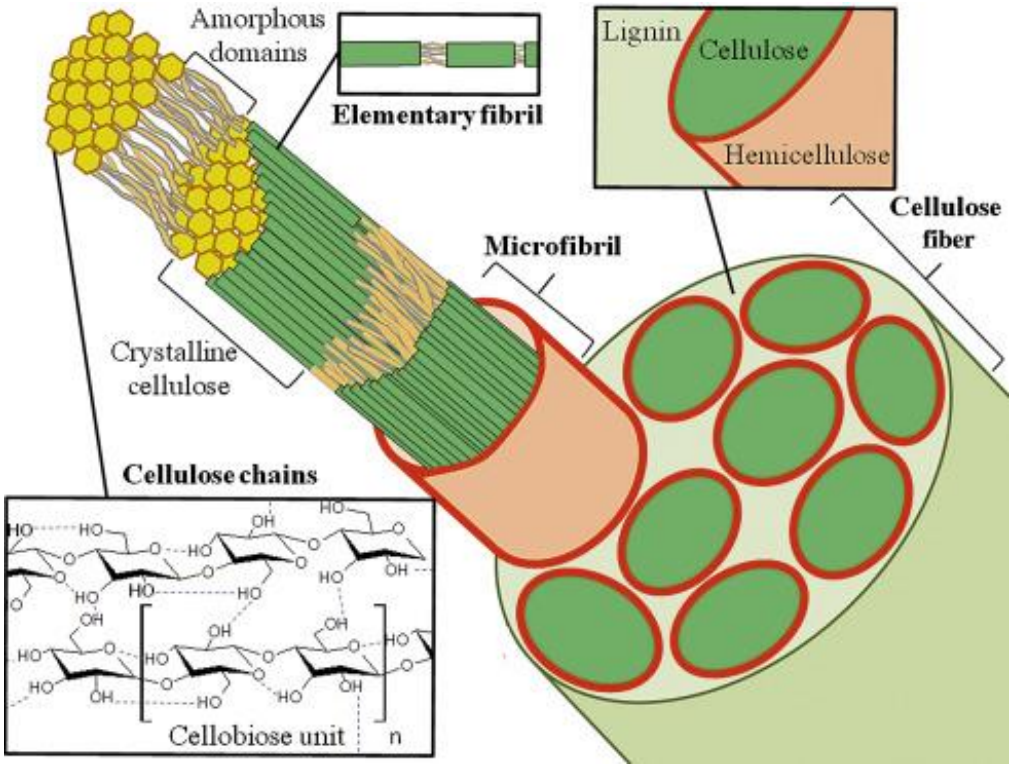

Figure 2.2 Structures of cellulose fibers (Arrieta et al., 2016).

2.2.2 Nanocellulose

Nanocellulose is the cellulose extract with a structure at a nanoscale (1-100 nm). It is derived from various types of sources, such as cotton, wood, bacteria, tunicates, and industrial biomass (Raghav et al., 2021). Nanocellulose are lightweight, biodegradable, and renewable. It is classified into three main groups, including cellulose nanocrystals (CNCs), cellulose nanofibrils (CNFs), and bacterial nanocellulose (BNC) (Raghav et al., 2021).

2.2.2.1 Cellulose nanocrystals

CNCs is a needle-shaped nanoparticle with a diameter of 10-30 nm and a length up to several hundred nanometers. CNCs are hydrophilic in nature and often synthesized through the hydrolysis of cellulose fibers by strong inorganic acid to remove amorphous regions but retain highly crystalline regions (**Figure 2.3**). Most used acids for the preparation of CNCs include sulphuric acid, phosphoric acid, and hydrochloric acid. CNCs obtained through sulphuric acid

hydrolysis possess a negatively charged surface due to the presence of sulfate half-ester groups, which plays a key role in stabilizing and dispersing CNCs in the suspension (Arrieta et al., 2016; Tian et al., 2016). CNCs own a high surface area-to-volume ratio, biocompatibility, and excellent mechanical properties (Islam et al., 2018; Du et al., 2019). To extract CNCs from cellulose fibers, a series of treatments are required. The pulp or fiber materials are often pre-treated with bleaching and sodium hydroxide (NaOH) to remove the non-cellulose portions, such as lignin and hemicellulose. After acid hydrolysis of cellulose fibers, several purification procedures, such as centrifugation and dialysis, are used to remove the remaining acids and any impurities. The final CNC products are obtained in either a suspension or powder form (Lee et al., 2019; Lin et al., 2019).

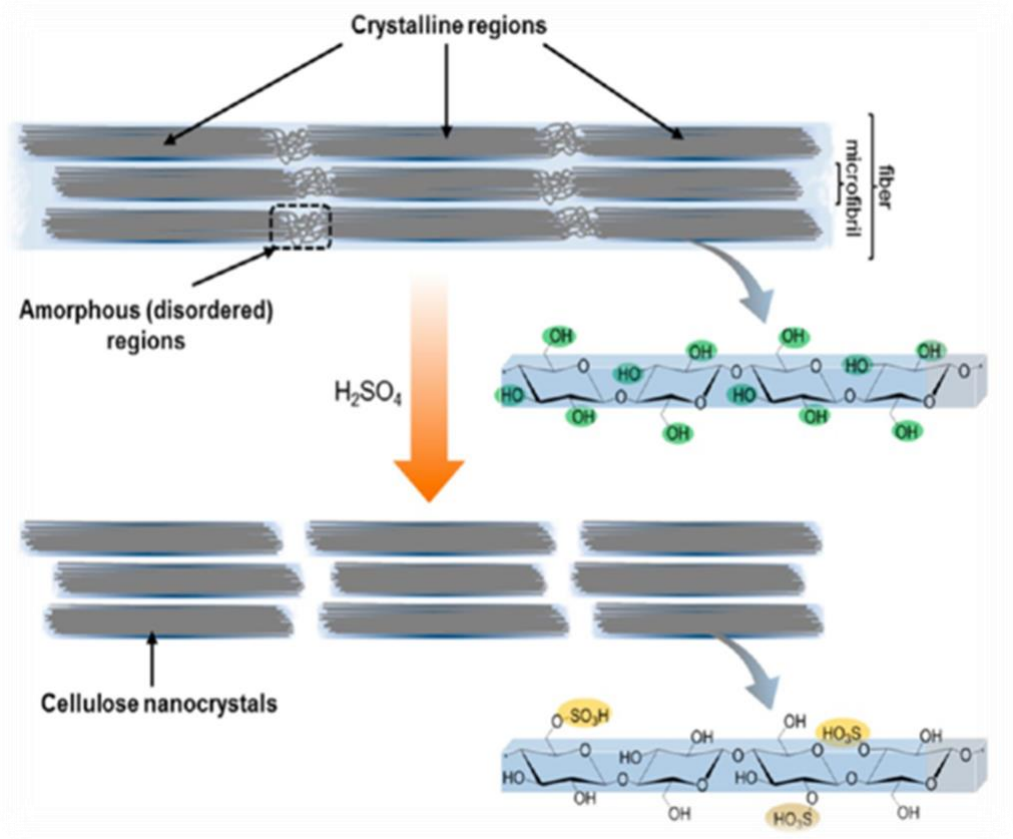

Figure 2.3 Synthesis of CNCs by sulfuric acid hydrolysis (Du et al., 2019).

2.2.2.2 Cellulose nanofibrils

CNFs are cellulose fibrils with a diameter of <100 nm and a length up to a few micrometers (500 nm–100 μm). Compared with CNCs, CNFs are less crystalline because their structures contain both amorphous and crystalline phases. CNFs have large surface area, good biodegradability, and can be obtained from wood and plant materials, such as hemp fibers, cassava peels, and wheat straws (Li et al., 2018; Raghav et al., 2021). CNFs are primarily produced through chemical, enzymatic, and mechanical methods. Chemical and enzymatic methods are often used as pre-treatments to separate cellulose fibrils. Mechanical processing is used to further reduce particle size to obtain CNFs (Du et al., 2019; Trache et al., 2020). For example, high pressure homogenization is a widely used mechanical method for the preparation of CNFs. Cellulose fibers are broken down through several homogenization cycles under high speed and high pressure to generate small and uniform CNFs (Tian et al., 2016). Anionization of cellulose through carboxymethylation or phosphorylation is commonly used in combination with high pressure homogenization to prepare CNFs. Phosphorylation of cellulose is achieved with the addition of phosphate and nitrogen-containing organic compounds, such as urea in the high oxygen state. Phosphorylated CNFs carry negative charges because of the presence of phosphate substitute hydroxyl groups, which largely reduce the cohesion between cellulose fibrils and impart CNFs enhanced flame retardancy and thermal resistance. In addition, cationization of cellulose introduces positive charges on CNFs through oxidization of hydroxyl groups on the surface by tertiary amines, quaternary ammonium groups, or gas plasma modifications. Cationization of CNFs can enhance the dispersion properties and antibacterial ability of cellulose fibrils (Yi et al., 2020). In comparison, 2,2,6,6-tetramethylpiperidine-1-oxyl (TEMPO)-mediated oxidation is considered as the most efficient and effective chemical treatment for the preparation of CNFs. As shown in **Figure 2.4**, TEMPO-oxidized CNFs are negatively charged due to the presence of carboxyl groups derived

from the oxidation of hydroxyl groups at the C_6 position. This surface modification can promote the dispersion of fibrils in suspension due to electrostatic interactions (Du et al., 2019; Huang et al., 2020).

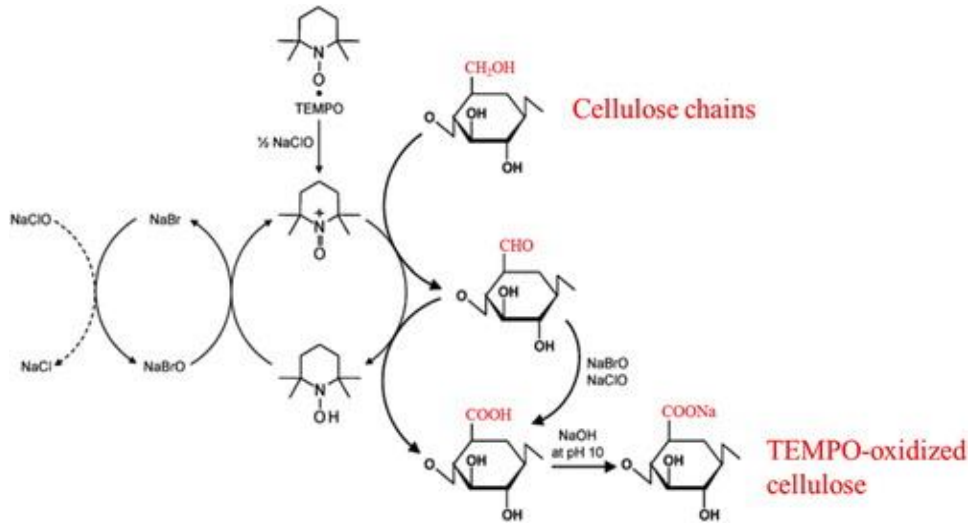

Figure 2.4 Schematic illustration of CNF synthesis by TEMPO-mediated oxidation (Isogai et al., 2011).

2.2.2.3 Bacterial nanocellulose

BNC is a natural cellulose fiber with a diameter of ~100 nm and a length up to a few hundred micrometers (Stanislawska, 2019). BNC can be produced by Gram-positive bacteria (*e.g., Sarcina ventriculi*) and Gram-negative bacteria (*e.g., Agrobacterium* and *Gluconacetobacter xylinus*) (Raghav et al., 2021). BNC-producing strains are often cultivated in media with glucose as the carbon source. BNC is a flexible, highly hydrated membrane with white color (Stanislawska, 2019; Krzyżek et al., 2020). BNC is a generally recognized as safe (GRAS) material approved by FDA and has excellent mechanical feature, water-holding ability, biocompatibility, high chemical purity, great flexibility, and remarkable absorbing property. BNC has been applied as materials for drug delivery and wound healing and for the generation of paper and textile products (Stanislawska, 2019; Sharma and Bhardwaj, 2019).

2.3 Antimicrobial modification of nanocellulose-based materials

Nanocellulose has great applications in developing novel nanocomposite materials due to its unique mechanical properties and surface chemistry. To further improve its potential for commercialization, antimicrobial nanocellulose-based materials have been developed for diverse applications, such as packaging materials, wound dressings, and drug carriers (Li et al., 2018; Tavakolian et al., 2020). Antimicrobial modifications of nanocellulose-based materials are summarized in this section.

2.3.1 Modification with quaternary ammonium compounds (QACs)

QACs have been used as antimicrobial agents, surfactants, and disinfectants for industrial and household purposes (Tischer et al., 2012). QACs are active cationic substances with a general structure of $N^{+}R_4X^{-}$, where R is the hydrogen atom, a plain alkyl group or alkyl group substituted with other functional groups and X represents an anion. The antimicrobial property of QACs relies on the length of the *N*-alkyl chain (Buffet-Bataillon et al., 2012). The lipophilic alkyl chains of QACs can bind to bacterial cell membrane, thereby reducing the permeability of cytoplasmic membrane and causing protein denaturation, disruption of enzyme activity, and leakage of cellular content (Hegstad et al., 2010; Tavakolian et al., 2020). Different QACs have been used for antimicrobial modifications of nanocellulose. For example, CNFs with the modification of glycidyl trimethyl ammonium chloride showed excellent antimicrobial properties against *Escherichia coli*, *Staphylococcus aureus*, and *Pseudomonas aeruginosa* (Chaker et al., 2015; Saini et al., 2016; Zhang et al., 2016). CNCs grafted with cationic porphrin displayed inhibitory effects against *S. aureus* and *Mycobacterium smegmatis* (Feeze et al., 2011; Li et al., 2018). Moreover, BNC grafted with aminoalkyl groups exhibited lethal effects on *E. coli* and *S. aureus* without causing remarkable cytotoxicity (Lu et al., 2004; Favi et al., 2013; Li et al., 2018).

2.3.2 *N*-halamine modification

N-halamines are biocidal compounds that contain one or more covalent bonds between nitrogen and halogen, which are formed via the halogenation of amine, imide, or amide groups. As shown in **Figure 2.5**, active halogens present in *N*-halamines can be chlorine, bromine, and iodine (Hui et al., 2013; Balaure and Grumezescu, 2020). *N*-halamine can inactivate a broad spectrum of microorganisms. Upon direct contact with bacteria, the nitrogen halogen bond of *N*-halamine will be broken to release oxidative halogens, which can disrupt the function of bacterial cell membrane by oxidizing the thiol or amino groups of proteins (Jiang et al., 2014; Cerkez, 2018; Tavakolian et al., 2020). For instance, CNCs grafted with 1-hydroxymethyl-5,5-dimethylhydantoin was incorporated in a film matrix made of chitosan and PVA. After chlorination, an antibacterial film was produced and exhibited inhibitory effects against *S. aureus* and *E. coli* O157:H7 (Zhang et al., 2019A; Zhang et al., 2019B). In addition, cotton cellulose was coated with 3-(3′-acrylicacidpropylester)-5,5-dimethylhydantoin (APDMH) and then chlorinated to generate a novel material that could efficiently inactivate *S. aureus* and *E. coli* O157:H7 (Li et al., 2015).

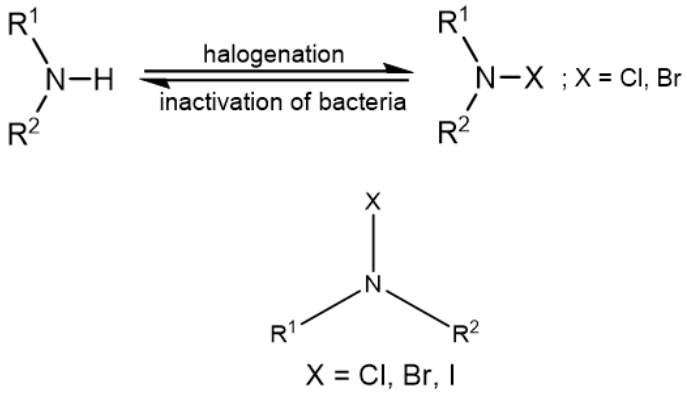

Figure 2.5 *N*-halamine chemical structure (Balaure and Grumezescu, 2020).

2.3.3 Modification with metal nanoparticles

Metal nanoparticles, such as silver nanoparticles (AgNPs) and gold nanoparticles (AuNPs), have strong antimicrobial ability against foodborne bacteria (Li et al., 2018; Gan and Chow et al., 2018). Metal nanoparticles are capable of releasing metal ions, which can interact with the negatively charged surface of bacteria and disrupt bacterial cell walls. In addition, the metal ions can enter bacterial cells, induce the production of reactive oxygen species (ROS) to increase the level of oxidative stress, and cause the damage of macromolecules within the cells (**Figure 2.6**) (Sánchez-López et al., 2020). AgNPs and AuNPs have been used to modify different types of nanocellulose, including CNCs, CNFs, and BNCs. CNC/AgNPs composites showed efficient antimicrobial ability against *E. coli*, multi-drug resistance *E. coli, S. aureus*, and methicillin-resistant *S. aureus* (Li et al., 2018; Errokh et al., 2019; Oun et al., 2020). BNC/AgNPs composites possessed porous structures, significant mechanical properties, water barrier capacity, and antimicrobial activities against *E. coli* and *S. aureus* (Li et al., 2018; Alavi, 2019). CNF/AgNPs composites were able to inhibit the growth of *P. aeruginosa*, *E. coli*, and *S. aureus* (Alavi, 2019). Moreover, AuNPs were incorporated in BNC to develop nanocomposites that showed stronger antimicrobial effects on *E. coli* and *P. aeruginosa* than antibiotics (Li et al., 2018). AuNPs-modified CNCs exhibited an inhibitory efficacy against *S. aureus*. It is noteworthy that cellulosic nanomaterials modified with metal nanoparticles have great potential for controlling multi-drug resistant bacteria (Van et al., 2017; Li et al., 2018; Su et al., 2020).

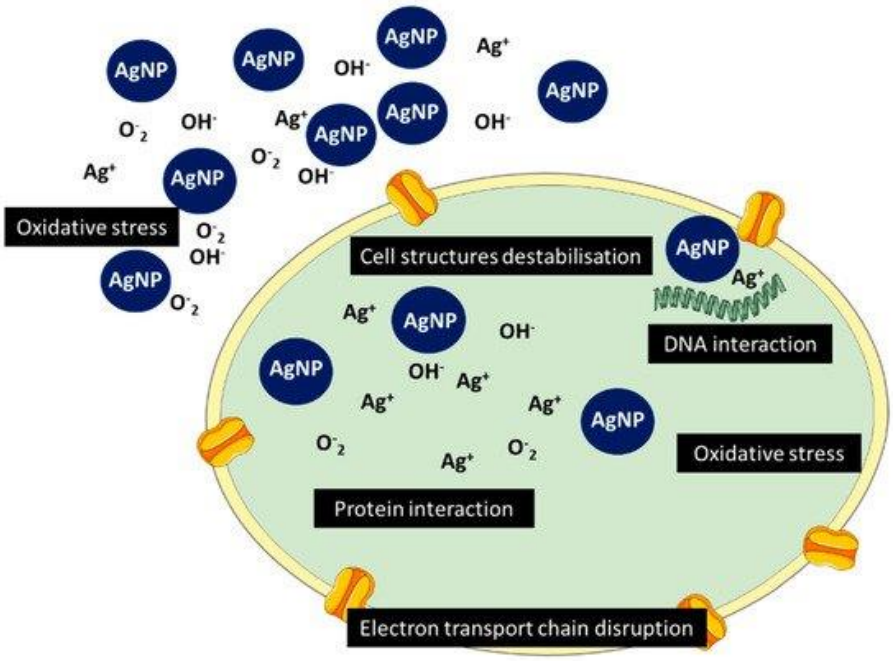

Figure 2.6 Antimicrobial mechanism of AgNPs (Sánchez-López et al., 2020).

2.3.4 Modification with metal oxide nanoparticles

Metal oxide nanoparticles can inactivate bacteria by attacking cell membrane, damage intracellular macromolecules (*e.g.*, protein and DNA), and disrupting the reproduction of bacteria (Gudkov et al., 2021). Metal oxide nanoparticles, such as zinc oxide nanoparticles (ZnO NPs) and copper oxide nanoparticles (CuO NPs), are often employed to improve the antimicrobial behavior of nanocellulose (Oun et al., 2020). For example, BNC pellicles were modified with ZnO NPs to produce BNC/ZnO NPs composites that could significantly inhibit the growth of *E. coli*, *Citrobacter freundii*, *P. aeruginosa*, and *S. aureus* (Oprea and Panaitescu, 2020). CNC/ZnO composites developed by using a hydrothermal method showed evident antibacterial activity against *E. coli* and *S. aureus* (Abdalkarim et al., 2018). Moreover, the BNC/CuO NPs composite was reported to show biocidal effects on *S. aureus*, *B. subtilis*, *E. coli*, and *P. aeruginosa* (Oprea and Panaitescu, 2020; Xie et al., 2020). Coating CuO NPs on CNFs resulted in composites that exhibited an inhibitory efficacy on the growth of *E. coli*, *S. aureus*, and *Candida albicans* (Muthulakshmi et al., 2017; Li et al., 2018; Oprea and Panaitescu,

2020). Nanostructures provided by nanocellulose played a critical role in preventing the agglomeration of CuO NPs and improving the stability of the resultant composites (Oun et al., 2020).

2.3.5 Modification with natural antimicrobial agents

2.3.5.1 Chitosan

Chitosan is a linear polysaccharide produced by deacetylation of chitin. Chitosan is biodegradable, nontoxic, and has antimicrobial activity. Low-molecular-weight chitosan can penetrate bacterial cell membrane and bind to nucleic acids to cause cell death, while high-molecular-weight chitosan can attach and accumulate on cell membrane to inhibit nutrient transportation. Chitosan has been used to improve antimicrobial capacity of nanocellulose-based materials (Sundaram et al., 2016; Li et al., 2018; Sivakanthan et al., 2020). CNC/chitosan composites showed biocidal effects on *E. coli* and *S. aureus* and were applied to improve the quality and safety of ground meat (Dehnad et al., 2014). BNC/chitosan composites were demonstrated as biodegradable, sustainable packaging materials with a high tensile strength, barrier properties, and notable antimicrobial efficacy against *E. coli* and *Aerococcus viridans*. Combining chitosan and nanocellulose in a film matrix can result in a novel antimicrobial material with the advantages of low cost and high biodegradability (Sharma et al., 2021).

2.3.5.2 Nisin

Nisin is an antimicrobial polypeptide that can be produced by *Lactococcus lactis*. Nisin can effectively inhibit the growth of Gram-positive bacteria through phospholipid bilayer destabilization by adhering to the surface of bacteria and forming transient pores. Since nisin is a GRAS material, it has great potential to be used in the food industry as food preservatives or antimicrobial agents to modify food packaging (Divsalar et al., 2018). For example, nisin

was incorporated in a film made of poly(lactic acid) (PLA) and CNCs to produce a composite film that exhibited inhibitory effects against *L. monocytogenes* in hams (Salmieri et al., 2014B). Additionally, nisin was used to modify a chitosan/cellulose composite to impart biocidal effects on *L. monocytogenes* in meat and dairy products.

2.3.5.3 Essential oil

Essential oil is a concentrated hydrophobic liquid from plant, which comprises a mixture of chemical compounds. Some essential oils containing antimicrobial compounds can cause bacterial cell wall lysis, leakage of cellular contents, damage of intracellular ATP pool, and cytoplasm coagulation. Antimicrobial essential oils are gaining increasing popularity for modification of nanocellulose-based composite materials (Sivakanthan et al., 2020). For instance, cinnamon essential oil has been added in a composite composed of sugar palm starch/CNCs (Syafiq et al., 2021). The resultant materials showed inhibitory efficacy against *B. subtilis*, *S. aureus*, and *E. coli*, and the antimicrobial activity is concentration-dependent. The composites exhibited significant antimicrobial effects along with the increase in essential oil concentration in the film matrix. In addition, oregano essential oil was incorporated into a film constructed by PLA and CNCs to form a nanocomposite film owing a strong antimicrobial activity against *L. monocytogenes* (Salmieri et al., 2014A).

2.3.5.4 Polylysine

Polylysine or epsilon-poly-L-lysine (ε-PL) is a cationic biopolymer composed of L-lysine residues linked by isopeptide bonds (**Figure 2.7**) (Hegde et al., 2018). It has advantages of being non-toxic, biodegradable, water-soluble, and thermally stable. In addition, it is a GRAS material approved by FDA and a natural antimicrobial that can inactive a wide range of Gram-positive and Gram-negative bacteria, such as *S. aureus*, *Bacillus coagulans*, *S.*

Typhimurium, and *E. coli* (You et al., 2017; Rodrigues et al., 2020). It can attach to the microbial surface and then change the integrity and permeability of cell membranes, thereby leading to rapid cell death (Najjar et al., 2007; Zhang et al., 2018; Tan et al., 2019). ε-PL has been grafted onto nanocellulose to impart antimicrobial ability. For example, TEMPO-oxidized CNFs were grafted with ε-PL to form a hydrogel that can effectively inhibit the growth of *E. coli* and *S. aureus* (Ren et al., 2022). This hydrogel also displayed high tensile strength, biocompatibility, and antioxidant ability. Moreover, BNC modified with ε-PL was capable of inhibiting the growth of *E. coli* and *S. aureus* through contact killing mechanism (Hyldgaard et al., 2014; Shahriari-Khalaji et al., 2022). So far, studies on antimicrobial modifications of nanocellulose by ε-PL are rarely reported yet.

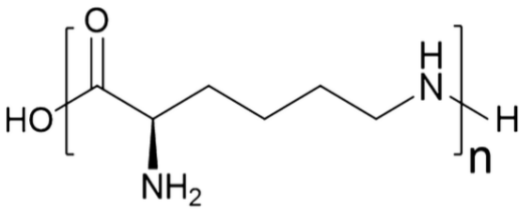

Figure 2.7 Chemical structure of polylysine (Hegde et al., 2018).

2.4 Nanocellulose in food packaging

2.4.1 Traditional food packaging

Food spoilage is a main cause of food wastage and often occurs during food transportation and storage and at the retailer and consumer levels. In the food industry, food packaging has been traditionally used to protect food products from microbial, chemical, and physical contamination and extend food shelf life (Brennan et al., 2020). However, most conventional food packaging is non-biodegradable and designed for single use. In Canada, only 20% of food packaging wastes are reused or recovered, while the rest of them end up in landfill

and pose a serious threat to the environment (Tiseo, 2018). In addition, since traditional food packaging is inert and not able to inhibit the growth of spoilage bacteria and foodborne pathogens, its antimicrobial capacity remains to be improved to meet the needs of consumers and industries (Salgado et al., 2021).

2.4.2 Active food packaging

Active food packaging is able to absorb or release substances from or into food packaging systems to offer extra functions (Han et al., 2018; Yildirim et al., 2018). There are two types of active packaging systems, including scavenging systems and releasing systems (**Figure 2.8**) (Yildirim, 2011). Active scavenging systems can absorb moisture, oxygen, ethylene, and carbon dioxide from the headspace of packaging. These systems apply absorbers or scavengers in sachets placed inside the packaging or incorporate active compounds into the packaging materials (Restuccia et al., 2010; Suppakul, 2015). Active releasing systems can release antioxidants, antimicrobials, carbon dioxide, flavor, and ethylene into the food products or the headspace of food packages (Han et al., 2018). Antimicrobial packaging is the most popular releasing systems because it can control microbial contamination and spoilage to improve food safety and quality (Yildirim and Röcker, 2018). Antimicrobial packaging performs inhibitory effects on microorganisms through either direct or indirect contact. The antimicrobial packaging that has direct contact with food products includes wrapping films and vacuum packages. Antimicrobials released by the packaging can migrate into food products to induce inhibitory effects. Some antimicrobial packaging materials do not have direct contact with foods but keep releasing active substances into the headspace of packages to create an environment that can inhibit the growth of microorganisms on food surface (Fang et al., 2017; Han et al., 2018). Most used antimicrobials in food packaging include essential oils, metal and metal oxide nanoparticles (*e.g.*, Ag NPs and ZnO NPs), chitosan, enzymes, and bacteriocins

(Yildirim et al., 2018). Active packaging systems, especially antimicrobial packaging systems, have been widely studied to extend food shelf life and reduce food waste and loss in the food supply chain (Fang et al., 2017).

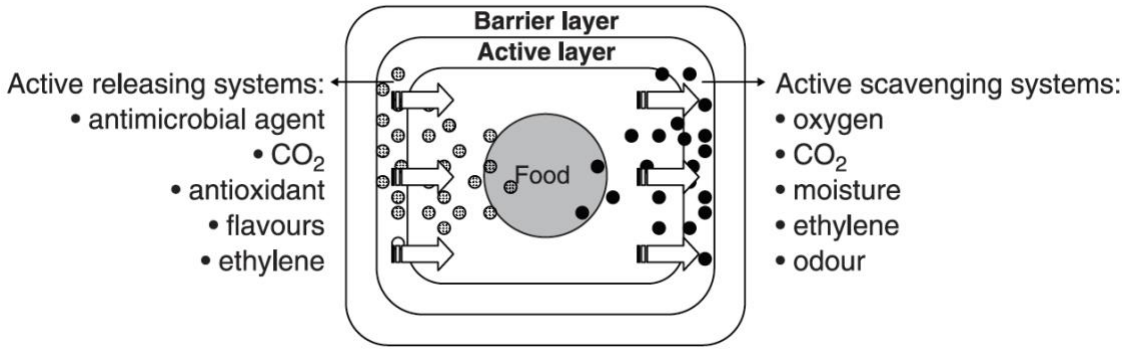

Figure 2.8 Schematic illustration of active food packaging systems (Yildirim, 2011).

2.4.3 Biodegradable packaging

Biodegradable packaging is the packaging that can break down and decompose naturally. Biodegradable packaging serves as an eco-friendly, sustainable packaging solution in the food industry due to its low environmental impact. This group of packaging is made of biopolymers and/or biodegradable synthetic polymers. Biopolymers include polysaccharides, proteins, and polyhydroxyalkanoates, while biodegradable synthetic polymers can be biomass-derived polymers (*e.g.*, PLA) or petroleum-derived polymers [poly(vinyl) alcohol (PVA)]. For example, with the addition of plasticizers, starch can be constructed into flexible thermoplastics with low cost, high biocompatibility, and transparency. Nevertheless, water vapor barrier capacity of starch films remains to be improved due to the hydrophilic nature of starch (Ribba et al., 2017; Salgado et al., 2021). PLA is a biomass-derived polymer prepared through the polymerization of lactic acid produced from the fermentation of the biomass rich in cellulose. PLA films are biodegradable, hydrophobic, and have been used as commercial packaging in the food industry. Drawbacks of PLA films center on poor thermal stability and gas barrier properties (Freeland et al., 2022). Moreover, PVA is a typical petroleum-derived polymer

because its synthesis involves the use of ethylene. PVA films are biodegradable, biocompatible, and has good gas barrier properties and mechanical performance. PVA-based packaging is not suitable for high-moisture foods because the material can uptake water, thereby causing decreases in water vapor barrier capacity and mechanical strength (Jain et al., 2018; Wang et al., 2018; Salgado et al., 2021).

2.4.4 Application of nanocellulose in food packaging

Within recent years, nanocellulose has gained growing popularity in the synthesis of bioplastics. This group of cellulosic nanomaterials can degrade into water and carbon dioxide through the activity of microorganisms in land and are advantageous of owning biodegradability, low toxicity, renewability, and thermal stability (Arrieta et al., 2016). Additionally, they can enhance mechanical performance and barrier properties of bioplastics against light, water vapor, and oxygen (Blanco et al., 2018). For example, after CNFs were added in starch/chitosan composites, the resultant films showed a significantly higher tensile strength and stiffness (Yu et al., 2017). Addition of CNFs also enhanced light and gas barrier properties of the composites, which could help retard food spoilage. In addition, nanocellulose carries abundant reactive hydroxyl groups on the surface, which can not only contribute to its remarkable compatibility in different composite film matrices but also allow it to be chemically modified to add desirable functionalities. For example, nanocellulose was incorporated into a chitosan/polylysine composite and showed excellent compatibility in the film matrix due to the formation of strong hydrogen bonds caused by the hydroxyl groups of nanocellulose (Wahid et al., 2019). Therefore, nanocellulose is considered as a promising material for the preparation of novel bioplastics for food packaging applications.

Overall, the cultivation and application of hemp plant in the industry are mainly focus on the processing of its seeds, leaves and flowers, while the hemp stalks have limited uses and

are treated as green waste. However, since the hemp stalk contains high cellulose content, it can be utilized as a desirable raw material for the extraction of wood nanocellulose including CNCs and CNFs. As mentioned in the previous studies, CNCs and CNFs can be added into food packaging as a filling material to render enhanced physical and biological properties. Nanocellulose is also a functional agent that can be well-cooperate with bioplastics such as PVA to form a commonly used packaging solution in food industry. In addition, polylysine can induce effective antimicrobial effects on CNFs, but the application about modification of nanocellulose by polylysine has not been widely studied yet. Thereby, the development of hemp nanocellulose-based bioplastic food packaging that be modified by polylysine could be feasible and will be investigated in this research project.

CHAPTER 3. MATERIALS AND METHODS

3.1 Materials

Hemp stalks were obtained from Costa Cana Corp. (Cowichan Vally, BC). Hemp bast fibers were manually peeled off from dried hemp stalks, and the rest part was used as hemp hurd. Ethanol (100% purity), sodium bisulfate ($NaHSO_4$; 99% purity), NaOH (≥97.0% purity), acetic acid (≥99.7% purity), sulphuric acid (H_2SO_4; 95.0-98.0% (w/w)), sodium chlorite ($NaClO_2$; ≥80% purity), sodium hypochlorite (NaClO; available chlorine 10-15%), 2,2,6,6-tetramethylpiperidine-1-oxyl (TEMPO; ≥98% purity), poly-L-lysine hydrochloride (PLH; M_w, >30,000 Da), PVA (M_w, 85,000-124,000 Da; ≥99% hydrolyzed), and glycerol (≥99.5% purity) were purchased from Sigma-Aldrich (St. Louis, MO, USA).

3.2 Extraction of hemp cellulose from hemp stalk

3.2.1 Extraction of hemp hurd cellulose

The hemp hurd fibers were ground by using a Moongiantgo multifunctional high-speed grinder (model, B0866X4YFP). The obtained powder was passed through a metal sieve (mesh size, 1.5 mm) and collected for cellulose extraction, which was conducted according to previous methods with some modifications (Luzi et al., 2014; Pacaphol and Aht-Ong, 2017). Briefly, the powder (50g) was treated by 12% (*w/v*) NaOH using a solid/liquid ratio of 1:15 at 80°C for 3 h with continuous stir at 500 rpm. The alkaline-treated sample was washed thoroughly by using deionized water for 4-5 times until a neutral pH was achieved. The alkaline treatment was repeated one more time to remove the remaining lignin, hemicellulose, and other impurities. Afterwards, the sample was bleached at 80°C for 4 h with continuous stir in a bleaching solution with a solid/liquid ratio of 1:15. The bleaching solution was prepared by mixing equal volume of an acetate buffer (54 g NaOH and 150 mL of acetic acid in 2 L of deionized water), 1.7% (*w/v*) $NaClO_2$ solution, and deionized water. The mixture was then

washed by deionized water for 4-5 times. The bleaching step was repeated for at least 3 times to obtain the cellulose fibers with a color close to white. Finally, the product was dried at 60°C in an oven overnight.

3.2.2 Extraction of hemp bast cellulose

Hemp bast fibers (30 g) were cut into small pieces (length, 1.5 cm) and treated by 12% (*w/v*) NaOH using a solid/liquid ratio of 1:25 at 80°C for 3 h with continuous stir at 500 rpm. The alkaline-treated sample was washed thoroughly by using deionized water for 4-5 times until a neutral pH was achieved. The alkaline treatment was repeated one more time to remove the remaining lignin, hemicellulose, and impurities. Moreover, the sample was bleached in a bleaching solution with a solid/liquid ratio of 1:20 at 80°C for 3 h with continuous stir. The mixture was washed with deionized water for 4-5 times. The sample was bleached again in a bleaching solution with a solid/liquid ratio of 1:20 at 80°C for 1 h with continuous stir at 200 rpm, followed by washing with deionized water for 4-5 times. The final product was dried at 60°C in an oven overnight.

3.2.3 Determination of chemical compositions

3.2.3.1 Determination of lignin content

The lignin content of samples was determined according to a reported method with some modifications (Song et al., 2019). In brief, samples (200 mg) were immersed in a H_2SO_4 solution (72%, *w*/*w*; 3 mL) at room temperature for 2 h. After deionized water (112 mL) was added, the mixture was boiled for 4 h and then vacuum-filtrated. The acid-insoluble lignin on the filter paper was oven-dried at 60°C overnight and weighed. The lignin content was calculated in mass fraction by dividing the obtained lignin mass by the initial sample mass.

3.2.3.2 Determination of hemicellulose content

The hemicellulose content of samples was determined according to a reported method with some modifications (Song et al., 2019). Briefly, 1 g sample was added into 30 mL of a mixture solution containing 0.25 mL of acetic acid, 0.3 g sodium chlorite, and deionized water. After the mixture was heated at 75°C for 1 h with continuous stir at 500 rpm, it was cooled down by running water, vacuum-filtrated, and washed with deionized water for at least three times. The obtained holocellulose was dried at 60°C in an oven overnight and weighed. Hemicellulose content can be calculated by subtracting cellulose content from holocellulose content.

3.2.3.3 Determination of cellulose content

The cellulose content of samples was determined according to a reported method with some modifications (Song et al., 2019). Hemp holocellulose collected from the previous procedures was treated with a 17.5% (*w*/*v*) NaOH solution at room temperature for 5 h with continuous stir at 500 rpm. The obtained cellulose was vacuum-filtrated and washed thoroughly with deionized water for 3 times. The obtained cellulose was oven-dried at 60°C overnight and weighed. The cellulose content was calculated by dividing the obtained cellulose mass by the initial sample mass.

3.2.4 Color determination

A CR-410 colorimeter was used to determine L^*, a^*, and b^* values of samples. The total color difference (ΔE) was calculated according to the following formula: $\Delta E = [(L^* - L_0^*)^2 + (a^* - a_0^*)^2 + (b^* - b_0^*)^2]^{1/2}$, where L^*, a^*, and b^* are color parameters obtained from samples, and L_0^*, a_0^*, and b_0^* are color parameters obtained from a calibration plate.

3.3 Preparation and characterization of hemp nanocellulose

3.3.1 Synthesis of hemp CNCs

CNCs were synthesized based on a reported method with some modifications (Luzi et al., 2014). Cellulose fibers were degraded using a 64% (*w/w*) sulfuric acid solution with a solid/liquid ratio of 1:8.75. The acid hydrolysis was conducted with continuous stir at 45°C for different time periods (30, 45, 60, 75, and 90 min). The reaction was stopped by the addition of deionized water (dilution factor, 20). The hydrolysate was centrifuged at 4,612 ×*g* for 10 min, and the resultant precipitant was collected and rinsed by deionized water. After another centrifugation at 4,612 ×*g* for 30 min, CNC suspension was dialyzed against distilled water for 10 d until a neutral pH was achieved. The final product was stored at 4°C for further use.

3.3.2 Synthesis of hemp CNFs

CNFs were synthesized based on a reported method with some modifications (Isogai et al., 2011). CNFs were prepared via the 2,2,6,6-tetramethylpiperidine-1-oxyl radical (TEMPO)-mediated oxidation method by oxidizing hydroxyl groups of cellulose fibers into carboxyl groups. The extracted hemp cellulose fibers were suspended in a solution dissolved with 0.016% (*w*/*v*) TEMPO and 0.1% (*w*/*v*) sodium bromide. The TEMPO-mediated oxidation was initiated by adding sodium hypochlorite (NaClO) with different concentrations (4, 8, and 12 mmol/g cellulose), respectively. The pH of the mixture was maintained at 10 with the addition of a 2% (*w*/*v*) NaOH solution until no pH change was observed. The CNF suspension was dialyzed for 7 d and stored at 4°C for further use.

3.3.3 Transmission electron microscopy (TEM)

The nanocellulose suspension was diluted to a concentration of 0.1 mg/g and then dropped on a S160 200-mesh copper/carbon grid (Agar Scientific, Parsonage Lane, Stansted,

UK). The copper/carbon grid was glow-discharged to create a positively charged surface on the grid. TEM micrographs were acquired using a Thermo Scientific Talos F200X G2 S/TEM at an accelerating voltage of 200 kV.

3.3.4 Zeta potential analysis

The zeta potential of samples (concentration, 0.1 - 0.2 mg/g) was determined by using the Brookhaven NanoBrook Omni particle sizer and zeta potential analyzer. For low-mobility samples, zeta potential was measured based on the phase analysis light scattering (PALS) measurement.

3.3.5 Determination of charge density

Conductometric titration was used to determine the amount of surface carboxyl groups of hemp CNFs (Jiang et al., 2013). CNF suspension (0.1%, *w*/*v*; 50 mL) was added with a 0.1M HCl solution to achieve a pH close to 2.5. Then, the mixture was titrated with 0.01M NaOH solution at the speed of 0.5 mL/30 s until the pH reached to 11. The conductivity value was recorded using a Fisherbrand™ accumet™ AB200 benchtop pH/conductivity meter. The density of surface carboxyl groups was indicated by the surface charge (σ, mmol/g of CNFs), which was calculated via the following equation: $\sigma = cv/m$, where c is NaOH concentration (M), m is the mass of CNFs in the suspension (g), v is the volume of NaOH consumed by titration.

3.4 Preparation and characterization of PVA/nanocellulose composite films

3.4.1 Synthesis of PVA/CNC composites

PVA was added in deionized water to reach to a concentration of 2% (*w/v*) and heated at 210°C with continuous stir until completely dissolved. Glycerol (30%, *w/w*, based on the

weight of PVA) was added and stirred for 15 min at room temperature. After CNCs (5%, 10%, and 20%, *w/w*, based on the weight of PVA) were added and well mixed, the film-making solution was cast into square petri dishes (120 mm × 120 mm) and air-dried at ambient temperature for 24 h. The films were peeled off from the petri dishes and stored at 50% RH at room temperature before further characterization. Four types of films were obtained, namely PVA film without CNCs (PVA), PVA film added with 5% CNCs (PVA/CNC5), PVA film added with 10% CNCs (PVA/CNC10), and PVA film added with 20% CNCs (PVA/CNC20).

3.4.2 Synthesis of PVA/CNF composites

PVA was added in deionized water to reach to a concentration of 2% (*w/v*) and heated at 210°C with continuous stir until completely dissolved. Glycerol (30%, *w/w*, based on the weight of PVA) was added and stirred for 15 min at room temperature. After CNFs (5%, 10%, and 20%, *w/w*, based on the weight of PVA) were added and well mixed, the film-making solution was cast into square petri dishes (120 mm × 120 mm) and air-dried at ambient temperature for 24 h. The films were peeled off from the petri dishes and stored at 50% RH at room temperature before further characterization. Four types of films were obtained, namely PVA film without CNFs (PVA), PVA film added with 5% CNFs (PVA/CNF5), PVA film added with 10% CNFs (PVA/CNF10), and PVA film added with 20% CNFs (PVA/CNF20).

3.4.3 Determination of mechanical properties

Tensile strength, elongation at break, and Young's modulus of film samples were evaluated using a ADMET MTESTQuattro materials testing system based on a previous method (Yu et al., 2017). The width and gauge length of each film were 5 and 30 mm, respectively. The stretching speed of the upper grip was set at 20 mm/min before its rupture.

3.4.4 Determination of light transmission and opacity

A Tecan Spark multimode microplate reader was used to determine the light transmission of film samples in the wavelength range of 200-800 nm. The absorbance of film samples at 600 nm was used to determine O value, a parameter that indicates film opacity (Siripatrawan and Harte, 2010). The O value was calculated with the following equation: $O = A_{600nm}/N$, where A_{600nm} is the absorbance of the film sample at 600 nm, and N is the film thickness (mm).

3.4.5 Scanning electron microscopy (SEM)

A FEI Quanta 450 environmental scanning electron microscope was used to observe the surface morphology of film samples. The samples were glued on aluminum stubs, sputter-coated with a thin layer of platinum (thickness, 4 nm), and then imaged using SEM.

3.5 Preparation and characterization of PVA/CNF/PLH composite films

3.5.1 Synthesis of PVA/CNF/PLH composite films

PVA was added in deionized water to reach to a concentration of 2% (*w/v*) and heated at 210°C with continuous stir until completely dissolved. Glycerol (30%, *w/w*, based on the weight of PVA) was added and stirred for 15 min at room temperature. After CNFs (10%, *w/w*, based on the weight of PVA) were added and well mixed, PLH (7.5% *w/w*, based on the weight of PVA) was added and stirred for 15 min. The film-making solution was cast into square petri dishes (120 mm × 120 mm) and air-dried at ambient temperature for 24 h. The films were peeled off from the petri dishes and stored at 50% RH at room temperature before further characterization. Three types of films were obtained, namely pure PVA film (PVA), PVA film added with 10% CNFs (PVA/CNF), and PVA film added with 10% CNFs and 7.5% PLH (PVA/CNF/PLH).

3.5.2 Characterization of nanocomposite films

Mechanical properties of film samples were determined based on the method described in subsection 3.4.3. Light transmission and opacity of film samples were determined based on the method described in subsection 3.4.4. Surface morphology of film samples was determined based on the method described in subsection 3.4.5. Fourier transformed infrared (FTIR) spectra of film samples were recorded using a Nicolet Summit Pro ATR-FTIR spectrometer within the wavenumber range of 4000–400 cm^{-1} at a resolution of 2 cm^{-1}. For obtaining a good signal-to-noise ratio, 32 scans were averaged and collected for each FT-IR spectrum.

3.5.3 Determination of antimicrobial effect

The films were cut into small circular pieces (diameter, 5 mm) and then placed on the agar plates inoculated with 150 μL of bacterial suspension (~10^8 CFU/mL). The bacterial suspension was diluted from the overnight culture grown at 37°C with shaking for 12 h. The antimicrobial capacity of each sample was determined after incubation at 37°C for 24 h under aerobic condition. Four types of bacteria were used in the antimicrobial test, including *Staphylococcus aureus* Newman, *Escherichia coli* K12, *Salmonella enterica* serotype Typhimurium SL1344, and *Pseudomonas aeruginosa* PA14. *S. aureus, E. coli*, and *S.* Typhimurium were separately grown in tryptic soy broth and plated on tryptic soy agar. *P. aeruginosa* was grown in Mueller-Hinton broth and plated on Mueller-Hinton agar (Yamada et al., 2011).

3.6 Statistical analysis

The experimental results were presented in terms of means ± standard deviation. Analysis of variance (ANOVA) was carried out for data analysis, and one-way multiple

comparison test by Duncan test was performed by using the SPSS Statistics software. A *P*-value of <0.05 was considered as significant.

CHAPTER 4. RESULTS AND DISCUSSION

4.1 Pre-treatment of hemp stalk

Hemp stalk was used as the raw material for cellulose extraction (**Figure 4.1a**). Hemp stalk was washed, air-dried, manually processed into bast and hurd fibers (**Figure 4.1b-d**) and then stored at room temperature for further processing.

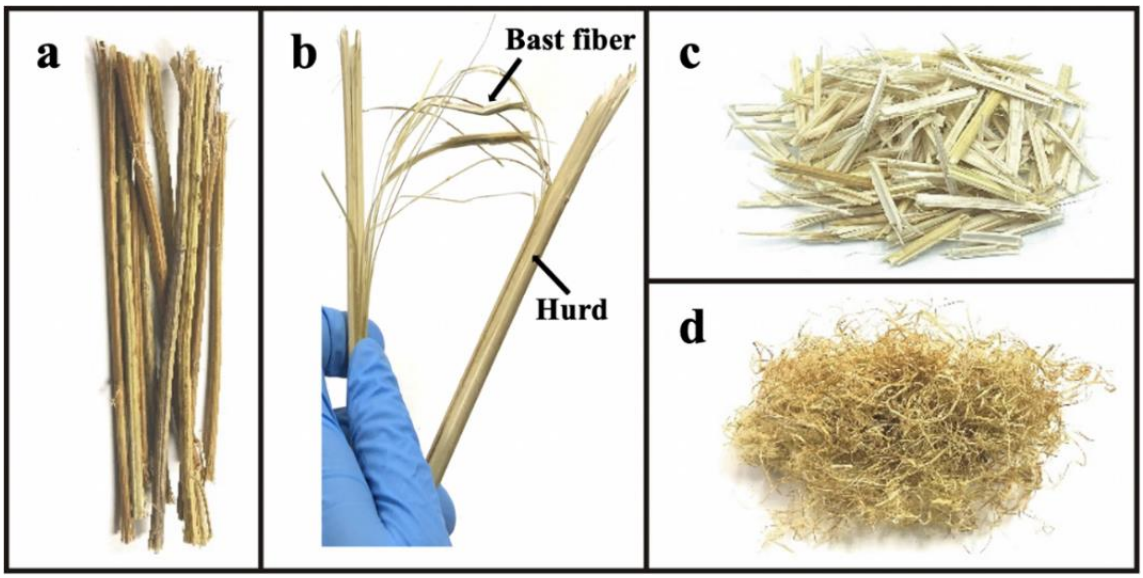

Figure 4.1 Photographs of hemp stalk used for cellulose extraction. (a) The hemp stalk offered by the industrial collaborator. (b) The hemp stalk with exposed bast fibers and hurds. (c) Hemp hurds used for cellulose extraction. (d) Hemp bast fibers used for cellulose extraction.

4.2 Hemp hurd cellulose

According to our experiments, the yield of hurd cellulose decreased with more alkaline or bleaching treatments applied for cellulose extraction. The extraction of hurd cellulose was optimized based on the purity and color of final products. As shown in **Figure 4.2**, after hemp hurd powder was processed with optimum alkaline and bleaching treatments, hurd cellulose was obtained in a lump form and showed a milky white color. The yield of hurd cellulose was determined to be 23.86%.

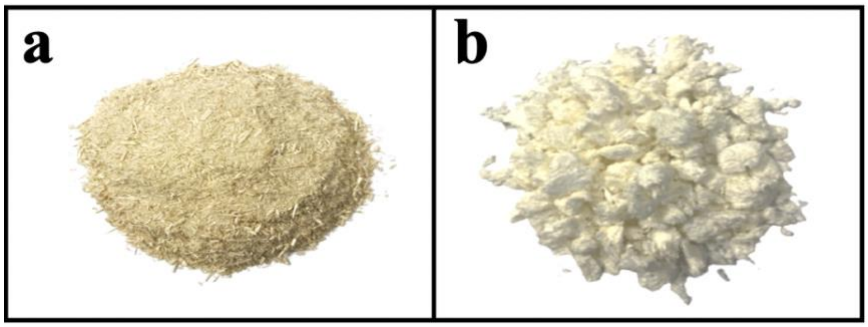

Figure 4.2 Photographs of hemp hurd powder (a) and extracted hurd cellulose (b).

Main components in hemp bast fibers and hurd include lignin, cellulose, and hemicellulose. As shown in **Table 4.1**, hemp hurd fibers had 20% cellulose and 17% lignin. The lignin content was close to the reported result (21%-24%), while the cellulose content was lower than the reported result (40%-48%) (Stevulova et al., 2014). This phenomenon was possibly due to the loss of cellulose caused by the pretreatment and the differences in growth conditions. After alkaline and bleaching treatments, the cellulose content was increased to 85%, and the levels of hemicellulose and lignin significantly decreased. Thus, most impurities were removed during the extraction process. The bleaching process produced several free radicals, such as hydroxyl free radicals and oxygen-derived free radicals, which could damage the chromophore of lignin. Meanwhile, the alkaline treatment effectively broke down the bonding between cellulose and lignin and solubilized hemicellulose, which promoted the release of cellulose from hemp hurd (Lee et al., 2009; Razali et al., 2022).

Table 4.1 Chemical composition of hemp hurd fibers and hurd cellulose.

Sample	Lignin (%)	Cellulose (%)	Hemicellulose (%)
Hurd fiber	16.53 ± 0.21	20.16 ± 0.14	63.22 ± 0.46
Hurd cellulose	1.35 ± 0.07	84.69 ± 0.99	9.96 ± 0.62

Each value is expressed as mean ± standard deviation (n = 3).

Thus, the color parameters of hurd cellulose were determined and listed in **Table 4.2**. The hurd cellulose had a high *L** value suggesting a color close to white. The positive *b** value indicate the yellowness of cellulose fibers, which was caused by the presence of lignin residues in the sample. The result was comparable to a previous study (Lee et al., 2020), which reported that removal of lignin and hemicellulose through the bleaching and alkaline treatments could significantly modify the yellow color of fibers in crop stalk.

Table 4.2 Color parameters of hemp hurd cellulose.

Color parameter	*L**	*a**	*b**
Hurd cellulose	87.11 ± 0.41	0.40 ± 0.14	3.37 ± 0.31

Each value is expressed as mean ± standard deviation (n = 3).

4.3 Hemp bast cellulose

Extraction of hemp cellulose was optimized based on the purity and color of final products. Hemp bast cellulose could be extracted in a less harsh conditions compared with hurd cellulose. As shown in **Figure 4.3**, hurd cellulose prepared under the optimum extraction condition showed a pure white color. The yield of hurd cellulose was determined to be 49.6%.

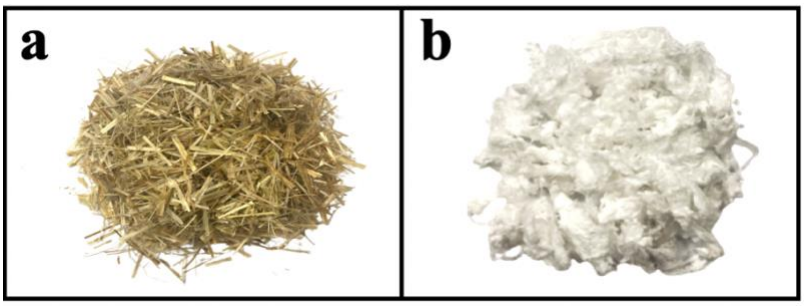

Figure 4.3 Photographs of hemp bast fibers (a) and extracted bast cellulose (b).

Chemical composition of hemp bast fibers and cellulose is summarized in **Table 4.3**. The cellulose content of hemp bast fibers was almost three times higher than that of hemp hurd.

In addition, hemp bast fibers showed a lower lignin and hemicellulose content compared with hemp hurd. After alkaline treatment and bleaching treatments, the final product achieved a high cellulose purity (97%), and its lignin and hemicellulose contents were controlled at a low level. Thus, hemp bast cellulose has a higher purity than hurd cellulose because hemp bast has a higher cellulose content but lower lignin and hemicellulose content. As a result, cellulose in hemp bast could be more easily released than cellulose in hemp hurd.

Table 4.3 Chemical composition of hemp bast fibers and bast cellulose.

Sample	Lignin (%)	Cellulose (%)	Hemicellulose (%)
Bast fiber	10.17 ± 0.29	65.91 ± 1.66	15.66 ± 1.52
Bast cellulose	0.92 ± 0.04	96.56 ± 0.25	1.86 ± 1.52

Each value is expressed as mean ± standard deviation (n = 3).

The color parameters of bast cellulose were determined and listed in **Table 4.4**. The *L** value of bast cellulose was higher than that of hurd cellulose, implying that bast cellulose displayed a whiter color than hurd cellulose. In addition, the *b** value of bast cellulose was close to zero and lower than that of hurd cellulose. After cellulose extraction, the yellowness of hemp bast disappeared due to the removal of lignin. Furthermore, hurd cellulose was yellower than bast cellulose because it contained a higher amount of lignin residues.

Table 4.4 Color measurement of hemp bast cellulose.

Color parameter	*L**	*a**	*b**
Sample	90.49 ± 0.18	0.097 ± 0.02	-0.35 ± 0.07

Each value is expressed as mean ± standard deviation (n = 3).

4.4 Hemp CNCs

Hemp CNCs were prepared by removing the amorphous regions of hemp bast cellulose by sulfuric acid for 30, 75, and 90 min, respectively. TEM images of hemp CNCs are shown in **Figure 4.4**. Regardless the hydrolysis time, CNC particles all showed a spindle-like shape and notable dispersity.

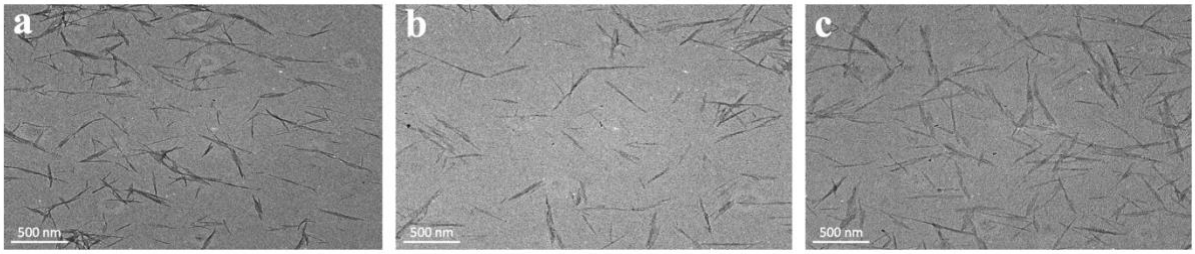

Figure 4.4 TEM images of hemp CNCs prepared by 30 min (a), 75 min (b), and 90 min (c) of acid hydrolysis.

The diameter, length, and aspect ratio of CNCs were calculated based upon the TEM images. As displayed in **Table 4.5**, hydrolysis time did not significantly affect the average diameter, length, and aspect ratio of CNC particles. When hydrolysis time was longer than 30 min, the particle size was not significantly changed. These results were comparable to those in the previous studies (Du et al., 2019; Kargarzadeh et al., 2012). Thus, hydrolysis time of 30 min was selected for CNC preparation. As shown in **Figure 4.5**, the suspension of CNCs prepared with 30 min of acid hydrolysis showed an ivory white color. Additionally, most CNCs had a diameter, length, and aspect ratio in the range of 10-35 nm, 100-450 nm, and 10-40, respectively. Thus, the prepared CNCs had a size at nanometer scale.

Table 4.5 Particle size of hemp CNCs.

Sample	Average diameter (nm)	Average length (nm)	Average aspect ratio
CNC-30 min	16.0 ± 7.4[a]	244.3 ± 100.7[a]	17.6 ± 8.9[a]
CNC-75 min	15.7 ± 5.6[a]	234.6 ± 95.1[a]	16.6 ± 8.7[a]
CNC-90 min	15.6 ± 5.7[a]	242.2 ± 97.3[a]	17.2 ± 9.0[a]

The data with different upper lowercase letters in each vertical column indicate the significant difference ($P < 0.05$).

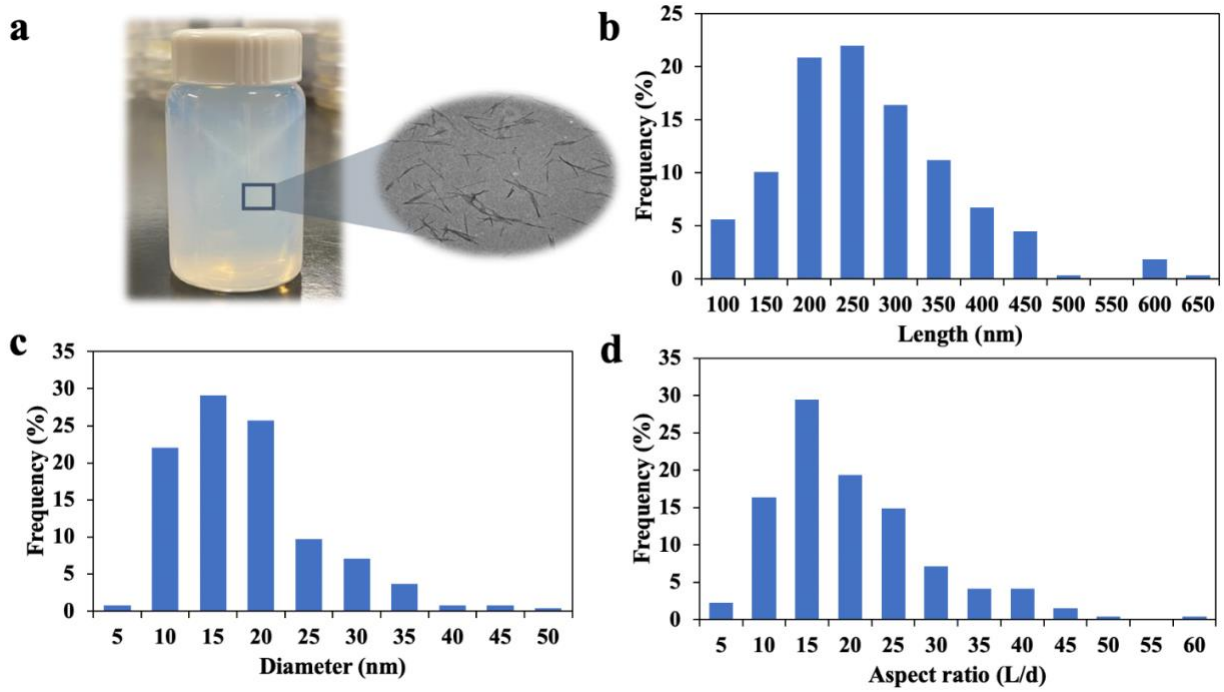

Figure 4.5 Photograph of hemp CNC suspension prepared by 30 min of acid hydrolysis (a) and the size distribution of CNCs in terms of length (b), diameter (c), and aspect ratio (d).

Zeta potential of CNCs was measured to determine the surface charges of these nanoparticles. As shown in **Table 4.6**, zeta potential values of CNCs were less than -48 mV. Thus, CNCs carried negative surface charges and this was derived from the sulfate half-ester groups formed due to sulfuric acid hydrolysis (Kargarzadeh et al., 2012). When zeta potential of a suspension is out of the range from -30 mV to 30 mV, the suspension is considered as a stable colloidal system because of the sufficient repulsive forces among particles (Angellier et al., 2005; Listyanda et al., 2020). Thus, the CNC suspensions prepared in this study had a high

colloidal stability and good dispersity. In addition, the CNCs prepared with longer acid hydrolysis time showed a lower zeta potential value. CNCs prepared with longer hydrolysis time can lead to the formation of more sulfate half-ester groups, which increased the negative charges on the surface of particles. As aforementioned, extension of hydrolysis time did not significantly influence the particle size. Generally, 30 min of acid hydrolysis was selected as the optimal condition to synthesize CNCs.

Table 4.6 Zeta potential of hemp CNCs.

Hydrolysis time	30 min	90 min
Zeta potential (mV)	-48.48 ± 1.24^{a}	-53.04 ± 1.45^{b}

The data with various upper lowercase letters in each vertical column indicate the significant difference ($P < 0.05$).

4.5 Hemp CNFs

The diameter, length, and aspect ratio of CNFs were calculated based upon the TEM images. As displayed in **Table 4.7**, all samples displayed an average diameter in the range of 15-24 nm. TEMPO-mediated oxidation was an effective approach to prepare CNFs. According to previous studies, the C_6 primary hydroxyl groups of cellulose were converted to C_6 carboxylate groups through TEMPO-mediated oxidation (Tarrés et al., 2017). The amount of NaClO added for oxidation could affect surface charge, fibrillation, and dispersity of the final CNF product (Patiño-Masó et al., 2019). Therefore, the effect of oxidation on the amount of carboxyl groups on CNFs was determined based on a titration method. As shown in **Table 4.8**, the surface charge density of CNFs showed an increasing trend along with a higher amount of NaClO added, indicating more carboxyl groups present on the surface of CNFs. Previous studies confirmed that the oxidation level of CNFs need to be well controlled. CNFs with a low oxidation level have limited fibrillation and dispersity. In comparison, CNFs with a high

oxidation level possess a low thermostability. Therefore, 8 mmol NaClO/g cellulose was selected for the preparation of CNF.

Table 4.7 Particle size of hemp CNFs.

Sample	Average diameter (nm)	Average length (nm)	Aspect ratio
CNF-4mmol	19.9 ± 7.3^{a}	298.2 ± 102.4^{a}	17.1 ± 10.65^{a}
CNF-8mmol	23.7 ± 10.7^{b}	292.4 ± 135.5^{a}	13.5 ± 6.9^{b}
CNF-12mmol	15.1 ± 4.9^{c}	187.2 ± 91.3^{b}	12.9 ± 5.8^{c}

The data with various upper lowercase letters in each vertical column indicate the significant difference ($P < 0.05$). Each value is expressed as mean ± standard deviation (n >100).

Table 4.8 Charge density of CNFs prepared with different amounts of NaClO.

Amount of NaClO (mmol/g cellulose)	4	8	12
Charge density (mmol/g cellulose)	0.52 ± 0.24^{a}	1.07 ± 0.11^{b}	1.72 ± 0.01^{c}

The data with various upper lowercase letters in each vertical column indicates the significant difference ($P < 0.05$). Each value is expressed as mean ± standard deviation (n = 3).

As shown in **Figure 4.6a**, purified and concentrated CNFs oxidized with 8 mmol NaClO/g cellulose were in a slurry form and displayed a white color. As observed in **Figure 4.6b**, CNFs showed nano-fibrillated structures with the diameter in a nanometer scale. Additionally, most CNFs had a diameter, length, and aspect ratio in the range of 10-60 nm, 100-650 nm, and 5-35, respectively (**Figure 4.7**). CNF product had a wider diameter and length range than CNC product because the oxidation could only affect the fibrillation of cellulose fibers, but the amorphous regions were retained.

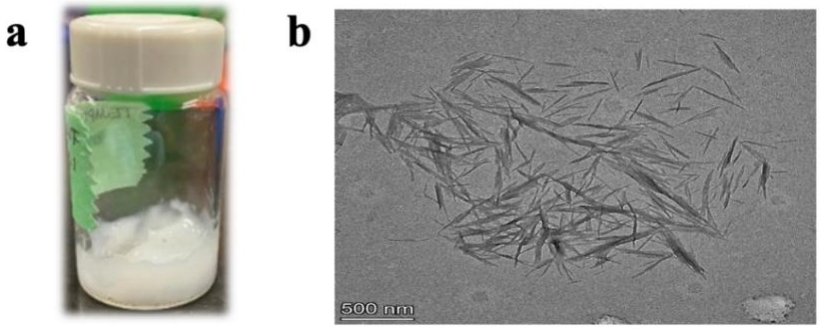

Figure 4.6 Photograph of CNF slurry in a glass bottle (a) and TEM image of CNF suspension prepared with 8 mmol NaClO/g cellulose (b).

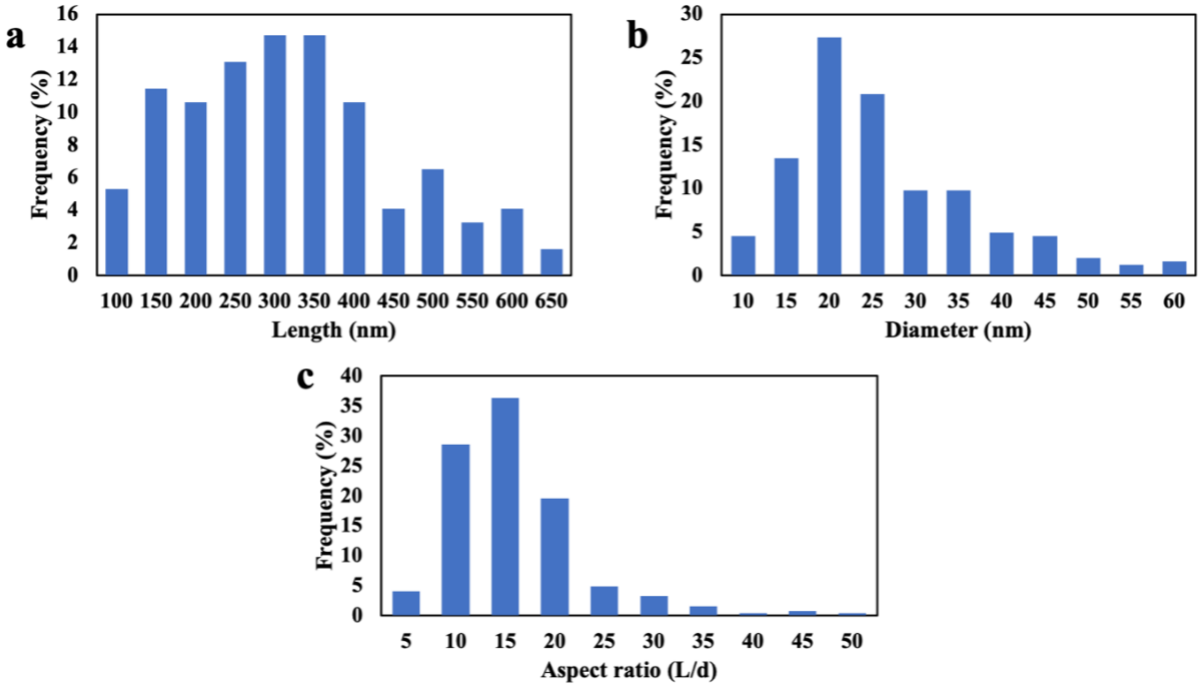

Figure 4.7 Size distribution of CNFs prepared by 8 mmol NaClO/g cellulose (a, length; b, diameter; and c, aspect ratio).

4.6 PVA/nanocellulose composite films

PVA is a synthetic polymer that has been applied by the food industry to develop biodegradable packaging. In this study, the PVA films were prepared using a casting method. As shown in **Figure 4.8**, PVA film was transparent and had a higher flexibility. Two different

types of hemp nanocellulose were incorporated into PVA films to prepare novel composites with improved mechanical and barrier properties.

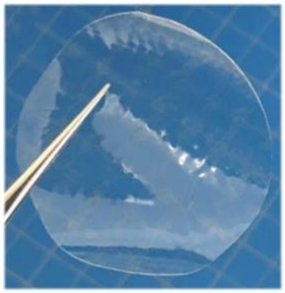

Figure 4.8 Photograph of a PVA film prepared using the casting method.

4.6.1 PVA/CNC composite films

Effects of hemp CNCs on tensile strength, elongation at break, and Young's modulus of composite films are shown in **Figure 4.9**. As displayed in **Figure 4.9a**, adding 5% and 10% of CNCs significantly improved the tensile strength of composites ($P < 0.05$), while the tensile strength decreased once CNC concentration reached to 20%. Addition of CNCs could provide more hydrogen bonds within the film matrix to improve the film strength (Jahan et al., 2018; Kim et al., 2019). If CNC content was too high, the interactions between PVA molecules would be disrupted, thereby resulting in a decrease in tensile strength. As shown in **Figure 4.9b**, incorporation of CNCs (5%-20%) did not cause a significant change in elongation at break. In addition, the addition of CNCs significantly enhanced the Young's modulus of composite films, and it was concentration-dependent (**Figure 4.9c**). Thus, CNCs could significantly increase the stiffness of PVA films. With more CNC added into the film matrix, the stiffness of composite film became stronger, which was comparable to the results reported in a previous study (Kim et al., 2019). The significant increase in Young's modulus was due to the high stiffness of CNCs and the strong interactions formed between PVA and CNCs that limited the mobility of polymers within the film.

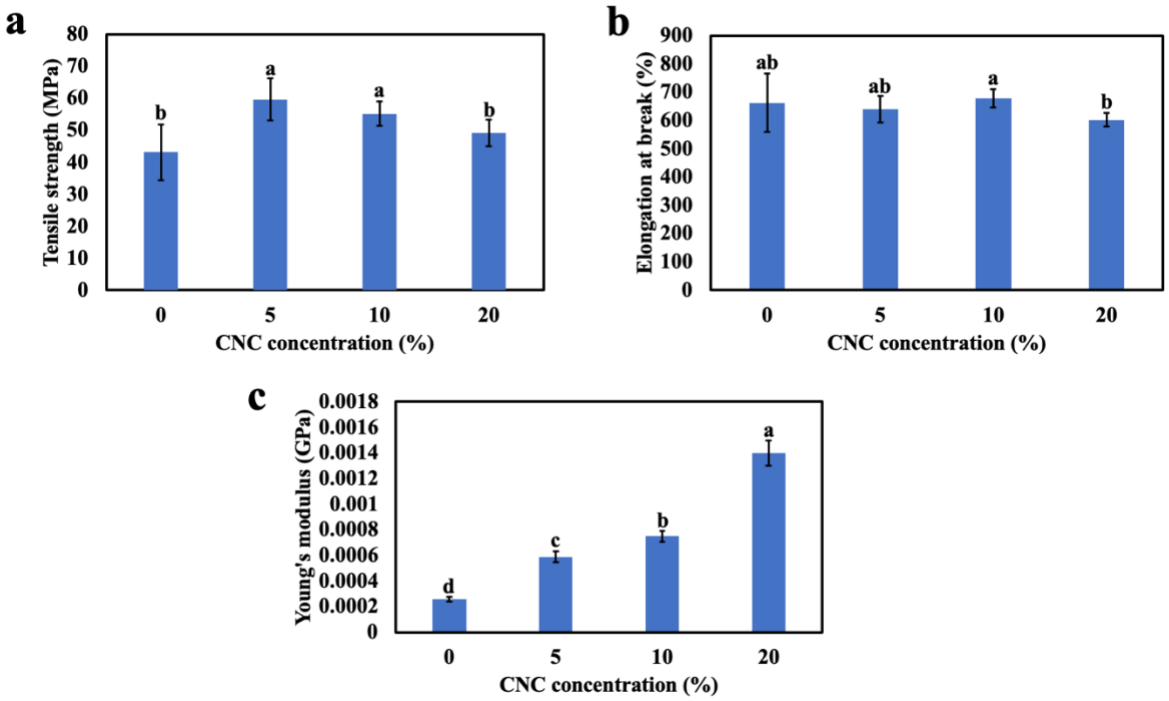

Figure 4.9 Effects of CNCs on the tensile strength (a), elongation at break (b), and Young's modulus (c) of composite films. The data with different lowercase letters are significantly different ($P < 0.05$).

Effects of hemp CNCs on the light barrier properties of composite films are shown in **Figure 4.10**. As shown in **Figure 4.10a**, addition of 5% CNCs in the PVA film significantly improved the opacity of composite films. Further addition of CNCs did not cause significant change in the film opacity ($P > 0.05$). As shown in **Figure 4.10b**, addition of CNCs evidently decreased the transmittance of composite films in the wavelength range of 200-400 nm. With more CNCs incorporated in the film, the transmittance of film samples exhibited a decreasing trend. Although the film opacity was increased with the incorporation of CNCs, the composite films still possessed a higher opacity. Moreover, the addition of CNCs can significantly decrease light transmission of the film in the wavelength range of ultraviolet. Since ultraviolet radiation is a key factor to cause food spoilage, the light barrier properties of PVA/CNC composite films can help extend the shelf life of food products (Moon et al., 2011; Silvério et al., 2013; Lizundia et al., 2017).

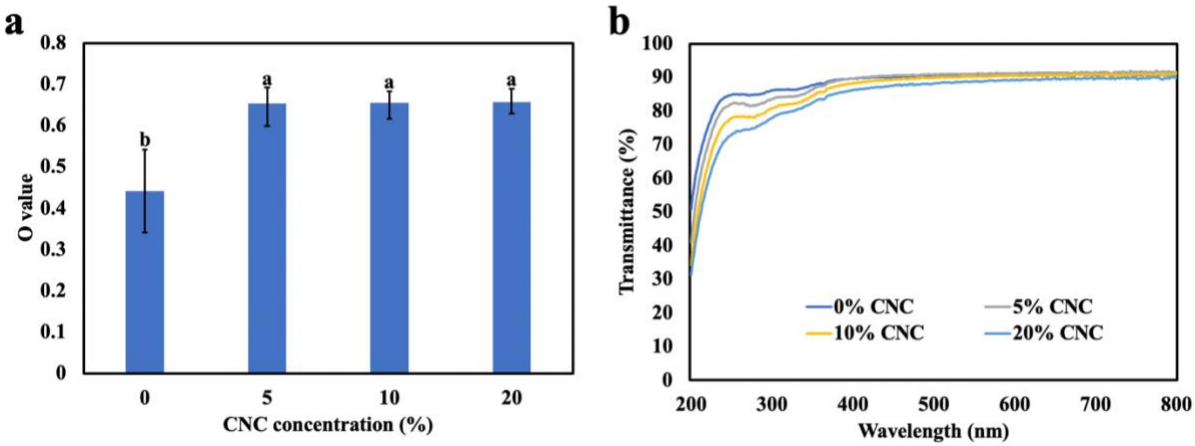

Figure 4.10 Effects of CNCs on the opacity (a) and transmission spectra (b) of composite films. In the panel (a), the data with different lowercase letters are significantly different ($P < 0.05$).

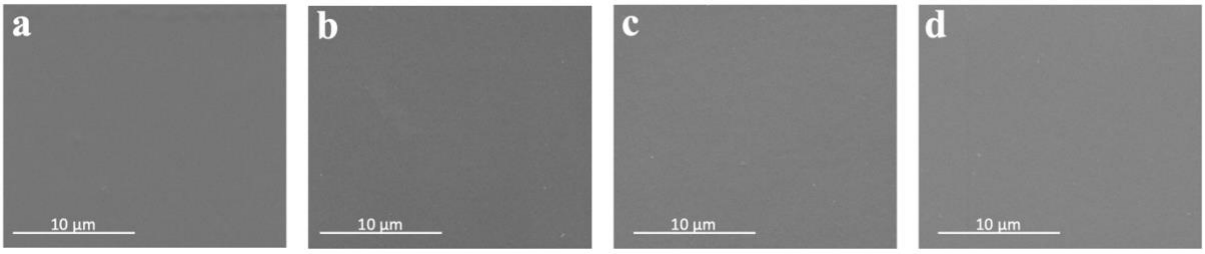

Figure 4.11 SEM observation of the surface of the PVA film (a) and PVA/CNC composite films (b, PVA/CNC5; c, PVA/CNC10; d, PVA/CNC20). Scale bar: 10 µm.

Effects of hemp CNCs on the surface morphology of composite films are shown in **Figure 4.11**. The surface of PVA films with and without CNCs all displayed flat, smooth surfaces. No cracks or pores were observed in the films. Incorporation of CNCs into PVA films did not cause significant change in film morphology. These results can be explained from two aspects. First, CNCs had a good miscibility with PVA and thus were well distributed in the film matrix. Second, incorporation of CNCs might restrict the crystallization of PVA molecules during film preparation, which promoted the homogeneity and smoothness of the composite films (Ben Shalom et al., 2019).

Based on the mechanical performance, light barrier properties, and surface morphology of composite films, the optimum amount of hemp CNCs added in PVA film was determined to be 10%.

4.6.2 PVA/CNF composite films

Effects of hemp CNFs on the tensile strength, elongation at break, and Young's modulus of composite films are shown in **Figure 4.12**. As displayed in **Figure 4.12a**, adding a low amount of CNFs improved the tensile strength of composite films, while the tensile strength decreased when the CNF concentration reached to 20%. As shown in **Figure 4.12b**, the incorporation of CNFs in PVA films significantly decreased their elongation at break. The lowest elongation at break was observed when 20% of CNFs were added. As shown in **Figure 4.12c**, the addition of CNFs significantly enhanced the Young's modulus of composite films, and it was concentration-dependent. Addition of CNFs could significantly increase the strength and stiffness of PVA films but decrease the film flexibility. The increased tensile strength is primarily derived from the formation of strong hydrogen bonds between PVA and CNFs, but adding an excess amount of CNFs could disrupt the interactions among PVA molecules and result in a decrease in tensile strength. Incorporation of CNFs in the PVA film gave rise to a denser network restricting the molecular motility of film components and thus led to a decrease in elongation at break (Nasri-Nasrabadi et al., 2014; Kim et al., 2019).

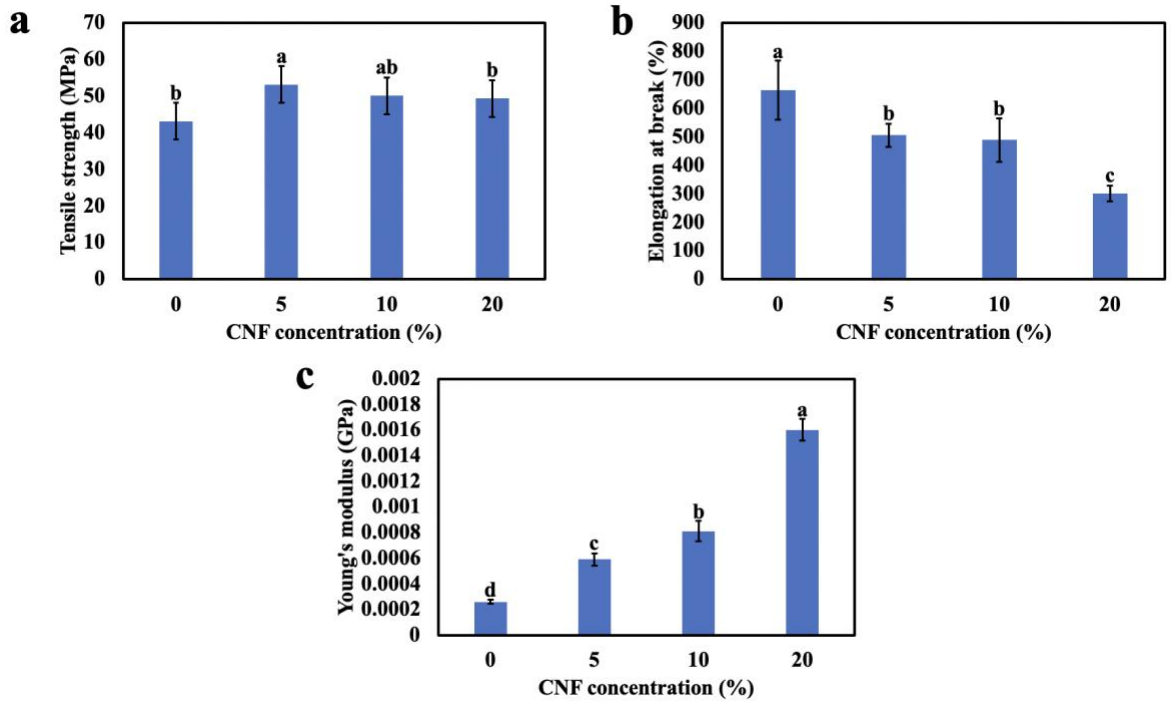

Figure 4.12 Effects of CNFs on the tensile strength (a), elongation at break (b), and Young's modulus (c) of composite films. The data with different lowercase letters are significantly different ($P < 0.05$).

Effects of hemp CNFs on the light barrier properties of composite films are shown in **Figure 4.13**. The addition of hemp CNFs evidently decreased the transmittance of composite films in the wavelength range of 200-400 nm. The most significant decrease was observed around 260 nm. With more hemp CNFs incorporated in the film, the transmittance of film samples exhibited a decreasing trend. Thus, addition of hemp CNFs could significantly decrease the transmittance of PVA films in the wavelength range of ultraviolet, while the transmittance in the visible light range (400-700 nm) was not notably changed. These results were consistent to those reported in the previous studies (Yu et al., 2017; Takahashi et al., 2009; Fukuzumi et al., 2013). In conclusion, hemp CNFs can help improve the light barrier properties of PVA films against ultraviolet.

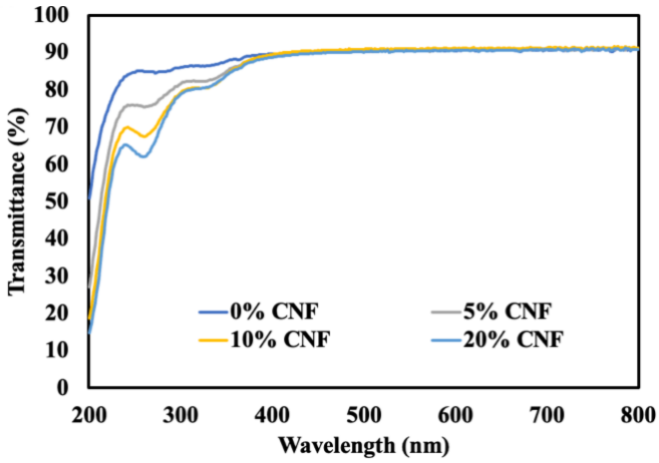

Figure 4.13 Effect of CNFs on the transmission spectra of composite films. The data with different lowercase letters are significantly different ($P < 0.05$).

Effects of hemp CNFs on the surface morphology of composite films are shown in **Figure 4.14**. The surface of PVA films with and without hemp CNFs all displayed flat and smooth surfaces. No cracks or pores were observed in the films. Incorporation of CNFs in the PVA films did not cause significant change in film morphology. Thus, hemp CNFs had a good compatibility with PVA films. CNFs were previously used as a filling material in packaging films. Adding a low amount of CNFs in biopolymer-based films could render a more compact film structure and reduce the pore size and number within the film (Yu et al., 2019a; Sánchez-Gutiérrez et al., 2021). When >20% of CNFs from sugarcane bagasse were added in the PVA film, fibrillated structures of CNFs were observed on the film surface (Somvanshi and Gope, 2021). These results were not in agreement with the data in the current study. One possible explanation was that the hemp CNFs had a better compatibility in the PVA film than CNFs from sugarcane bagasse.

Based on the mechanical performance, light barrier properties, and surface morphology of composite films, the optimum amount of hemp CNFs added in the PVA film was determined to be 10%.

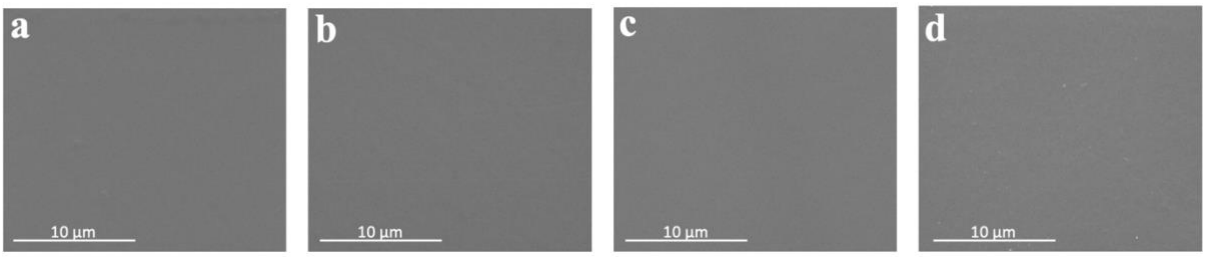

Figure 4.14 SEM observation of the surface of the PVA film (a) and PAV/CNF composite films (b, PVA/CNF5; c, PVA/CNF10; d, PVA/CNF20). Scale bar: 10 µm.

4.7 PVA/CNF/PLH composite films

In the previous section, it was demonstrated that hemp CNFs had a good compatibility with PVA films and could enhance their mechanical performance and light barrier properties. However, based on our experiments, the PVA/CNF composite films are inert and not able to show antimicrobial effect to improve food safety and shelf life. Therefore, PLH, a biodegradable antimicrobial, was incorporated in the PVA/CNF composite with the goal to produce a novel material for antimicrobial food packaging.

4.7.1 Film appearance

The photographs of PVA and composite films are shown in **Figure 4.15**. As seen in **Figure 4.15a**, the PVA film showed a great transparency. Appearance of the PVA film was not significantly changed after the addition of CNFs or PLH. Thus, PVA, CNFs, and PLH were miscible in water. Additionally, the remarkable transparency of the PVA/CNF/PLH film would allow the consumers to see food products clearly through the packaging film (Ma et al., 2011; Yu et al., 2019b).

Figure 4.15 The appearance of PVA (a), PVA/CNF (b), and PVA/CNF/PLH (c) films with the background of McGill logo.

4.7.2 Mechanical properties

Mechanical properties of PVA and composite films are shown in **Figure 4.16**. Addition of CNFs in PVA film led to increases in tensile strength and Young's modulus and a decrease in elongation at break. After further incorporation of PLH, the tensile strength and elongation at break of the composite film decreased. Thus, addition of CNFs made PVA film stronger, stiffer, and less flexible, which was identical to the results in the previous section. In addition, loading PLH in the composite film caused reduced flexibility and strength. Previous studies identified that PLH could alter the crystal structure of CNFs, disrupt the film matrix, and thus reduce the strength of composite films (Zhu et al., 2010). PLH was also able to induce cross-linking with PVA and CNFs in the film matrix through hydrogen bonds, which could mitigate the mobility of film components and weaken the film flexibility (Wahid et al., 2019).

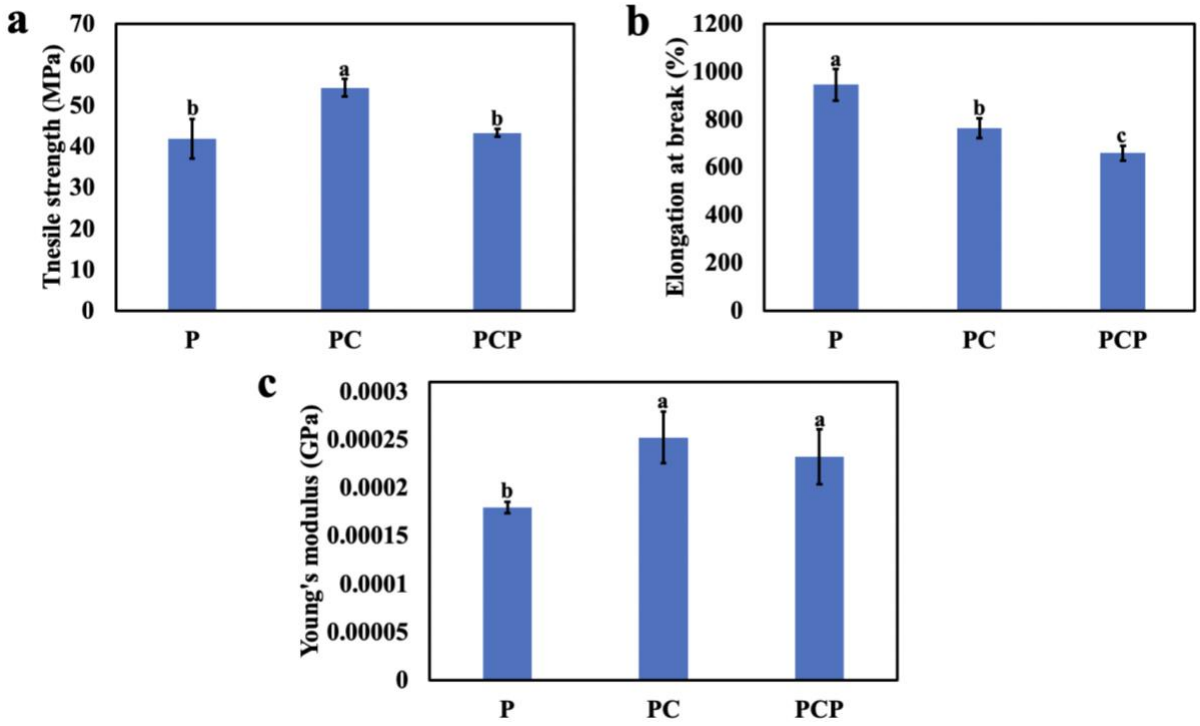

Figure 4.16 Mechanical performance of PVA and composite films (a, tensile strength; b, elongation at break; c, Young's modulus). The data with different lowercase letters are significantly different ($P < 0.05$). P, PC, and PCP indicate PVA, PVA/CNF, and PVA/CNF/PLH films, respectively.

4.7.3 Light barrier properties

Light barrier properties of PVA and composite films are shown in **Figure 4.17**. With the addition of hemp CNFs, the transmittance of PVA film decreased, especially in the wavelength range from 200-350 nm. When PLH was incorporated, the film transmittance was further reduced. Thus, adding hemp CNFs improved the light barrier properties of PVA films, which was in agreement with the results in the previous section. Addition of PLH also decreased the light transmission of PVA film, especially in the wavelength range of ultraviolet. A previous study reported a similar result that adding ε-PL into a PVA/bacterial cellulose composite film led to the decrease in transmittance in the wavelength range of 200-800 nm (Wahid et al., 2019). This was because ε-PL could form hydrogen bonds among PVA

molecules and cellulose fibers, which disrupted the crystalline structure of the film matrix and therefore increased the barrier capacity against light.

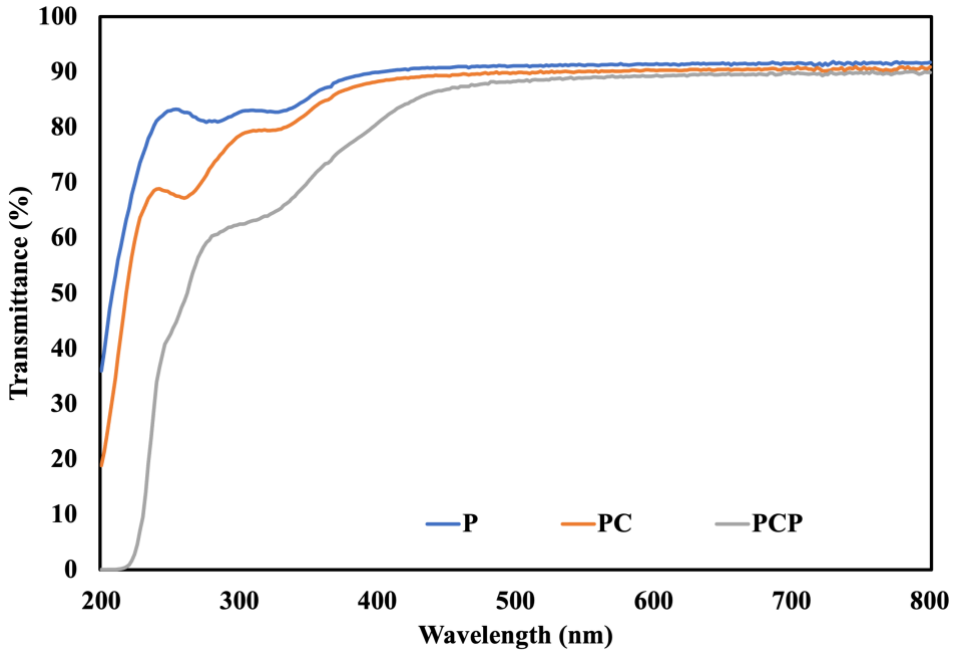

Figure 4.17 Transmission spectra of PVA and composite films. P, PC, and PCP indicate PVA, PVA/CNF, and PVA/CNF/PLH films, respectively.

4.7.4 Surface morphology

SEM images of PVA and composite films were obtained to observe the surface morphology of film samples. As shown in **Figure 4.18**, addition of CNFs in PVA films did not cause a notable change in surface morphology. When PLH was added in the film, the surface of the composite maintained a flat and smooth structure. No cracks or pores were observed in PVA and composite films. Thus, CNFs had a good filling effect in PVA film, and PLH had a remarkable compatibility with the film components. A previous study reported a similar result that addition of CNFs did not change surface morphology of a PVA-based film (Wahid et al., 2019). The authors also identified that addition of nanocellulose increased the roughness of film surface, which was different from the results in the current study. One explanation was

that glycerol was added as a plasticizer to enhance the miscibility of polymers in the film (Li et al., 2020).

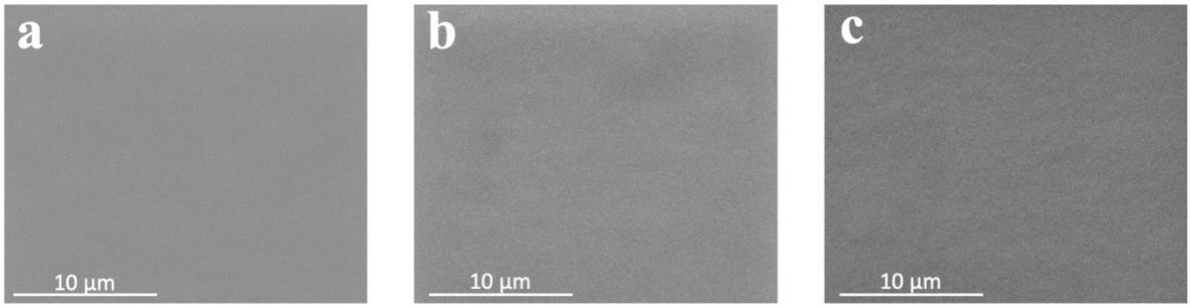

Figure 4.18 SEM micrographs of the surface of PVA (a), PVA/CNF (b), PVA/CNF/PLH (c) films. Scale bar: 10 µm.

4.7.5 FTIR spectra

FTIR spectra of PVA and composite films are shown in **Figure 4.19**. For the PVA film, two broad peaks at 3255 and 2939 cm^{-1} were displayed, representing O–H stretching and C–H stretching, respectively. The bands at 1326 and 1089 cm^{-1} were attributed to C–H bending and C–O stretching (Dmitrenko et al., 2018; Jahan et al., 2018). The peak at 1654 cm^{-1} was due to C=O stretching derived from the acetate groups in PVA molecule (Thomas et al., 2001). With the addition of hemp CNF, the peak due to O–H stretching was shifted to 3269 cm^{-1}, indicating the formation of hydrogen bonds among CNFs and PVA (Wu et al., 2019). With the incorporation of PLH, two strong peaks appeared at 1649 and 1546 cm^{-1}, which were attributed to C=O stretching vibration in the amide I region and N–H bending in the amide II region, respectively. These groups were derived from the peptide bonds in PLH molecule (Gao et al., 2014). In addition, the peak due to O–H stretching was shifted to 3274 cm^{-1}, which was caused by the generation of hydrogen bonds among PLH, PVA, and CNFs (Wahid et al., 2019). Thus, addition of CNFs and PLH in PVA film largely enhanced hydrogen bonds formed in the film matrix.

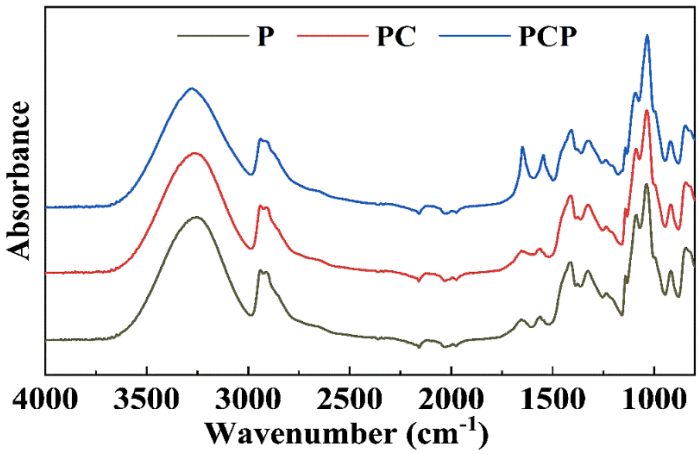

Figure 4.19 FTIR spectra of PVA and composite films. P, PC, and PCP indicate PVA, PVA/CNF, and PVA/CNF/PLH films, respectively.

4.7.6 Antimicrobial effect of composite films

Antimicrobial effects of PVA and composite films are shown in **Figure 4.20**. Inhibitory effects of film samples on Gram-positive and Gram-negative bacteria were determined on the agar plates. PVA and PVA/CNF films showed a milky white color on the agar plate inoculated with *S.* Typhimurium, *S. aureus*, *E. coli*, and *P. aeruginosa*. Both Gram-positive and Gram-negative bacteria were able to grow after covered by PVA and PVA/CNF films. In addition, the agar plates covered by PVA/CNF/PLH film were transparent, indicating that the growth of bacteria was significantly inhibited through contact inhibition (Hyldgaard et al., 2014; Tan et al., 2019). The results in this study were comparable to those reported in the previous studies that both PVA and CNFs do not have antimicrobial activities (Hu and Wang, 2016; Tavakolian et al., 2020). ε-PL was added in different biopolymer-based films and exhibited inhibitory effects on *E. coli*, *S. aureus*, *S.* Typhimurium, *P. aeruginosa*, *Bacillus subtillis*, and *Aspergillus niger* (Zhang et al., 2018; Tan et al., 2019; Georgnaras et al., 2007; Wei et al., 2017). The antimicrobial ability of ε-PL was because of its positively charged amine groups that could change the integrity and permeability of bacterial membrane and inactivate bacterial cells

(Zhang et al., 2018; Tan et al., 2019). Due to the presence of PLH, the PVA/CNF/PLH composite film was able to inhibit the growth of bacteria through direct contact.

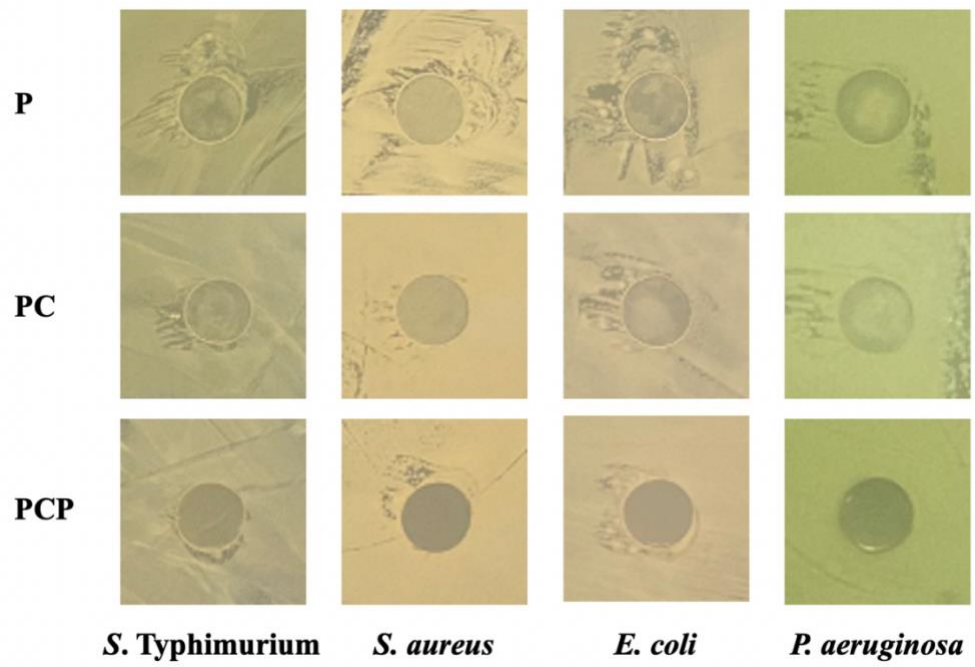

Figure 4.20 Antimicrobial effect of P, PC, and PCP films on the agar plates inoculated with *S.* Typhimurium, *S. aureus*, *E. coli*, and *P. aeruginosa*. P, PC, and PCP indicate PVA, PVA/CNF, and PVA/CNF/PLH films, respectively.

CHAPTER 5. CONCLUSION

In this thesis project, hemp stalk, a waste produced in the hemp industry, was successfully converted into value-added products, including hemp CNCs and CNFs. The optimum conditions to extract cellulose from hemp hurd and bast fibers were determined on the basis of repeated alkaline and bleaching treatments. Hemp bast cellulose was selected as the raw material for the synthesis of hemp nanocellulose due to its high cellulose content (97%) and yield (49.6%). Hemp CNCs were synthesized through sulfuric acid hydrolysis for 30 min. The CNC product had a high colloidal stability in aqueous suspension and had an average diameter of 16 nm and an average length of 244 nm. Hemp CNFs were produced by the TEMPO-mediated oxidation with the addition of 8 mmol of NaClO/g cellulose. The CNF product had a high dispersity and possessed an average diameter of 24 nm and an average length of 292 nm. Application of hemp nanocellulose in developing biodegradable composite films was demonstrated in different film matrix. Hemp CNCs showed a good compatibility in a PVA film, and the addition of 10% CNCs significantly improved the strength, stiffness, and ultraviolet-blocking effect of PVA film. Likewise, hemp CNFs were miscible with PVA in the composite film. When 10% CNFs were added, the PVA film displayed increased strength, stiffness, and ultraviolet-blocking effect. In addition, hemp CNFs, PLH, and PVA were used to develop a novel composite film. The film owned a high transparency, good mechanical performance, UV-blocking effect, and antimicrobial activities against Gram-positive and Gram-negative bacteria. The PVA/CNF/PLH film was biodegradable, sustainable, and had great potential to be used as an antimicrobial packaging to improve food quality and safety.

Future studies should be addressed from the following three perspectives. First, more novel nanocomposite films incorporated with hemp nanocellulose will be developed. In this study, hemp nanocellulose was used as a filler in the PVA-based films. In the next step, it is necessary to incorporate hemp nanocellulose in the films made of other biodegradable

polymers, such as poly(lactic acid) and starch. Second, the antimicrobial activity of the PVA/CNF/PLH film should be further investigated in a food model. Since the PVA/CNF/PLH film was identified to inhibit the growth of both Gram-positive and Gram-negative bacteria via contact inhibition, the film had potential to be used for food packaging. Therefore, the antimicrobial effect of the composite in a food model, such as poultry and red meat, should be evaluated. Third, the PVA/CNF/PLH film should be produced at a larger scale. In this work, all the composite films were prepared using a casting method, which was only suitable for making films at a laboratory scale. For this reason, the technologies to prepare the PVA/CNF/PLH film at a pilot scale should be explored through extrusion or thermocompression in future.

REFERENCES

Abdalkarim, S. Y. H., Yu, H. Y., Wang, C., Yang, L., Guan, Y., Huang, L., & Yao, J. (2018). Sheet-like cellulose nanocrystal-ZnO nanohybrids as multifunctional reinforcing agents in biopolyester composite nanofibers with ultrahigh UV-shielding and antibacterial performances. *ACS Applied Bio Materials*, *1*, 714-727.

Alavi, M. (2019). Modifications of microcrystalline cellulose (MCC), nanofibrillated cellulose (NFC), and nanocrystalline cellulose (NCC) for antimicrobial and wound healing applications. *e-Polymers*, *19*, 103-119.

Angellier, H., Putaux, J. L., Molina-Boisseau, S., Dupeyre, D., & Dufresne, A. (2005, January). Starch nanocrystal fillers in an acrylic polymer matrix. In *Macromolecular Symposia* (Vol. 221, No. 1, pp. 95-104). Weinheim: WILEY-VCH Verlag.

Arrieta, M. P., Fortunati, E., Burgos, N., Peltzer, M. A., Lopez, J., & Peponi, L. (2016). Chapter 7 - Nanocellulose-Based Polymeric Blends for Food Packaging Applications, *Multifunctional Polymeric Nanocomposites Based on Cellulosic Reinforcements* (pp. 205-252). Elsevier Inc.

Balaure, P. C., & Grumezescu, A. M. (2020). Recent advances in surface nanoengineering for biofilm prevention and control. Part II: active, combined active and passive, and smart bacteria-responsive antibiofilm nanocoatings. *Nanomaterials*, *10*(8), 1527.

Ben Shalom, T., Nevo, Y., Leibler, D., Shtein, Z., Azerraf, C., Lapidot, S., & Shoseyov, O. (2019). Cellulose nanocrystals (CNCs) induced crystallization of polyvinyl alcohol (PVA) super performing nanocomposite films. *Macromolecular Bioscience*, *19*(3), 1800347.

Blanco, A., Monte, M. C., Campano, C., Balea, A., Merayo, N., & Negro, C. (2018). Chapter

5 - Nanocellulose for Industrial Use: Cellulose Nanofibers (CNF), Cellulose Nanocrystals (CNC), and Bacterial Cellulose (BC), *Handbook of Nanomaterials for Industrial Applications* (pp. 74-126).

Brennan, L., Langley, S., Verghese, K., Lockrey, S., Ryder, M., Francis, C., Phan-le, N. T., & Hill, A. (2020). The role of packaging in fighting food waste: A systematised review of consumer perceptions of packaging. *Journal of Cleaner Production*, *281*, 125276.

Buffet-Bataillon, S., Tattevin, P., Bonnaure-Mallet, M., & Jolivet-Gougeon, A. (2012). Emergence of resistance to antibacterial agents: the role of quaternary ammonium compounds—a critical review. *International Journal of Antimicrobial Agents*, *39*(5), 381-389.

Cerkez I. (2018). 18 - N-Halamine-Based Antimicrobial Coatings, *Handbook of Antimicrobial Coatings* (pp. 391-409). Elsevier Inc.

Chaker, A., & Boufi, S. (2015). Cationic nanofibrillar cellulose with high antibacterial properties. *Carbohydrate Polymers*, *131*, 224-232.

Charrette, A., Akingbasote, J., Guthrie, N., & Hilmas, C. J. (2021). Chapter 39 – Cannabidiol Safety, *Nutraceutical: Efficacy, Safety and Toxicity (2nd ed.)* (pp. 625-659). Elsevier Inc.

Chen, J. H., Liu, J. G., Su, Y. Q., Xu, Z. H., Li, M. C., Ying, R. F., & Wu, J. Q. (2019). Preparation and properties of microfibrillated cellulose with different carboxyethyl content. *Carbohydrate Polymers*, *206*, 616-624.

Cheng, L., Ren, S., & Lu, X. (2020). Application of eco-friendly waterborne polyurethane composite coating incorporated with nano cellulose crystalline and silver nano particles on wood antibacterial board. *Polymers*, *12*, 407.

Dehnad, D., Mirzaei, H., Emam-Djomeh, Z., Jafari, S. M., & Dadashi, S. (2014). Thermal and

antimicrobial properties of chitosan–nanocellulose films for extending shelf life of ground meat. *Carbohydrate Polymers*, *109*, 148-154.

Divsalar, E., Tajik, H., Moradi, M., Forough, M., Lotfi, M., & Kuswandi, B. (2018). Characterization of cellulosic paper coated with chitosan-zinc oxide nanocomposite containing nisin and its application in packaging of UF cheese. *International Journal of Biological Macromolecules*, *109*, 1311-1318.

Dmitrenko, M. E., Penkova, A. V., Kuzminova, A. I., Morshed, M., Larionov, M. I., Alem, H., ... & Roizard, D. (2018). Investigation of new modification strategies for PVA membranes to improve their dehydration properties by pervaporation. *Applied Surface Science*, *450*, 527-537.

Du, H., Liu, W., Zhang, M., Si, C., Zhang, X., & Li, B. (2019). Cellulose nanocrystals and cellulose nanofibrils based hydrogels for biomedical applications. *Carbohydrate Polymers*, *209*, 130-144.

Dufresne, A. (2019). Nanocellulose Processing Properties and Potential Applications. *Current Forestry Reports*, *5*, 76–89.

Errokh, A., Magnin, A., Putaux, J. L., & Boufi, S. (2019). Hybrid nanocellulose decorated with silver nanoparticles as reinforcing filler with antibacterial properties. *Materials Science and Engineering: C*, *105*, 110044.

Fang, Z., Zhao, Y., Warner, R. D., & Johnson, S. K. (2017). Active and intelligent packaging in meat industry. *Trends in Food Science & Technology*, *61*, 60-71.

Farinon, B., Molinari, R., Costantini, L., & Merendino, N. (2020). The seed of industrial hemp (Cannabis sativa L.): Nutritional quality and potential functionality for human health and nutrition. *Nutrients*, *12*(7), 1935.

Favi, P. M., Benson, R. S., Neilsen, N. R., Hammonds, R. L., Bates, C. C., Stephens, C. P., &

Dhar, M. S. (2013). Cell proliferation, viability, and in vitro differentiation of equine mesenchymal stem cells seeded on bacterial cellulose hydrogel scaffolds. *Materials Science and Engineering: C*, *33*(4), 1935-1944.

Feese, E., Sadeghifar, H., Gracz, H. S., Argyropoulos, D. S., & Ghiladi, R. A. (2011). Photobactericidal porphyrin-cellulose nanocrystals: synthesis, characterization, and antimicrobial properties. *Biomacromolecules*, *12*(10), 3528-3539.

Freeland, B., McCarthy, E., Balakrishnan, R., Fahy, S., Boland, A., Rochfort, K. D., ... & Gaughran, J. (2022). A Review of Polylactic Acid as a Replacement Material for Single-Use Laboratory Components. *Materials*, *15*(9), 2989.

Fukuzumi, H., Saito, T., & Isogai, A. (2013). Influence of TEMPO-oxidized cellulose nanofibril length on film properties. *Carbohydrate Polymers*, *93*(1), 172-177.

Gan, I., & Chow, W. S. (2018). Antimicrobial poly (lactic acid)/cellulose bionanocomposite for food packaging application: A review. *Food packaging and shelf life*, *17*, 150-161.

Gao, C., Yan, T., Du, J., He, F., Luo, H., & Wan, Y. (2014). Introduction of broad spectrum antibacterial properties to bacterial cellulose nanofibers via immobilising ε-polylysine nanocoatings. *Food Hydrocolloids*, *36*, 204-211.

Gao, Y., & Li, D. (2020). Preparation and characterization of corn starch/PVA/glycerol composite films incorporated with ε-polylysine as a novel antimicrobial packaging material. *e-Polymers*, *20*(1), 154-161.

Georgnaras, I., Yoon, Y., Belk, K. E., Smith, G. C., & Sofos, J. N. (2007). Antimicrobial activity of ε-polylysine against Escherichia coli O157: H7, Salmonella typhimurium, and Listeria monocytogenes in various food extracts. *Journal of Food Science*, *72*(8), M330-M334.

Gudkov, S. V., Burmistrov, D. E., Serov, D. A., Rebezov, M. B., Semenova, A. A., & Lisitsyn,

A. B. (2021). A Mini Review of Antibacterial properties of ZnO nanoparticles. *Fronters in Physics, 9,* 641481.

Han, J.-W., Ruiz-Garcia, L., Qian, J.-P., & Yang, X.-T. (2018). Food packaging: a comprehensive review and future trends. *Comprehensive Reviews in Food Science and Food Safety, 17,* 860-877.

Hegde, N., Velingkar, V., & Prabhakar, B. (2019). An update on design and pharmacology of dendritic poly (l-lysine). *International Journal of Peptide Research and Therapeutics*, *25*(4), 1539-1562.

Hegstad, K., Langsrud, S., Lunestad, B. T., Scheie, A. A., Sunde, M., & Yazdankhah, S. P. (2010). Does the wide use of quaternary ammonium compounds enhance the selection and spread of antimicrobial resistance and thus threaten our health. *Microbial Drug Resistance*, *16*(2), 91-104.

Hu, D., & Wang, L. (2016). Physical and antibacterial properties of polyvinyl alcohol films reinforced with quaternized cellulose. *Journal of Applied Polymer Science, 133*(25).

Huang, P., Zhang, P., Min, L., Tang, J., & Sun, H. (2020). Synthesis of cellulose carbon aerogel via combined technology of wet ball-milling and TEMPO-mediated oxidation and its supersorption performance to ionic dyes. *Bioresource Technology, 315,* Article 123815.

Hui, F., & Debiemme-Chouvy, C. (2013). Antimicrobial N-halamine polymers and coatings: a review of their synthesis, characterization, and applications. *Biomacromolecules*, *14*(3), 585-601.

Hyldgaard, M., Mygind, T., Vad, B. S., Stenvang, M., Otzen, D. E., & Meyer, R. L. (2014). The antimicrobial mechanism of action of epsilon-poly-l-lysine. *Applied and Environmental Microbiology*, *80*(24), 7758-7770.

Islam, M. S., Chen, L., Sisler, J., & Tam, K. C. (2018). Cellulose nanocrystal (CNC)–inorganic

hybrid systems: synthesis, properties and applications. *Journal of Materials Chemistry B, 6*, 864-883.

Jahan, Z., Niazi, M. B. K., & Gregersen, Ø. W. (2018). Mechanical, thermal and swelling properties of cellulose nanocrystals/PVA nanocomposites membranes. *Journal of Industrial and Engineering Chemistry*, *57*, 113-124.

Jain, N., Singh, V. K., & Chauhan, S. (2017). A review on mechanical and water absorption properties of polyvinyl alcohol based composites/films. *Journal of the Mechanical Behavior of Materials*, *26*(5-6), 213-222.

Jiang, F., Han, S., & Hsieh, Y. L. (2013). Controlled defibrillation of rice straw cellulose and self-assembly of cellulose nanofibrils into highly crystalline fibrous materials. *RSC Advances*, *3*(30), 12366-12375.

Jiang, Z., Ma, K., Du, J., Li, R., Ren, X., & Huang, T. S. (2014). Synthesis of novel reactive N-halamine precursors and application in antimicrobial cellulose. *Applied Surface Science*, *288*, 518-523.

Karche, T. & Singh, R. (2019). The application of hemp (*Cannabis sativa* L.) for a green economy: a review. *Turkey Journal of Botany, 43*, 710-723.

Kargarzadeh, H., Ahmad, I., Abdullah, I., Dufresne, A., Zainudin, S. Y., & Sheltami, R. M. (2012). Effects of hydrolysis conditions on the morphology, crystallinity, and thermal stability of cellulose nanocrystals extracted from kenaf bast fibers. *Cellulose*, *19*(3), 855-866.

Kargarzadeh, H., Ahmad, I., Thomas, S., & Dufresne, A. (Eds.). (2017). *Handbook of nanocellulose and cellulose nanocomposites, 2 volume set*. John Wiley & Sons.

Khan, M. R., Chen, Y., Lague, C., Landry, H., Peng, Q., & Zhong, W. (2010). Compressive properties of Hemp (*Cannabis sativa* L.) stalks. *Biosystems Engineering*, *116*, 315-323.

Kim, J. W., Park, H., Lee, G., Jeong, Y. R., Hong, S. Y., Keum, K., ... & Ha, J. S. (2019). Paper-like, thin, foldable, and self-healable electronics based on PVA/CNC nanocomposite film. *Advanced Functional Materials*, *29*(50), 1905968.

Krzyżek, P., Gościniak, G., Fijałkowski, K., Migdał, P., Dziadas, M., Owczarek, A., ... & Junka, A. (2020). Potential of bacterial cellulose chemisorbed with anti-metabolites, 3-bromopyruvate or sertraline, to fight against helicobacter pylori lawn biofilm. *International Journal of Molecular Sciences*, *21*(24), 9507.

Lee, H. J., Lee, H. S., Seo, J., Kang, Y. H., Kim, W., & Kang, T. H. K. (2019). State-of-the-art of cellulose nanocrystals and optimal method for their dispersion for construction-related applications. *Applied Sciences*, *9*(3), 426.

Lee, S. C., Yoo, E., Lee, S. H., & Won, K. (2020). Preparation and application of light-colored lignin nanoparticles for broad-spectrum sunscreens. *Polymers*, *12*(3), 699.

Lee, Y. J., Chung, C. H., & Day, D. F. (2009). Sugarcane bagasse oxidation using a combination of hypochlorite and peroxide. *Bioresource Technology*, *100*(2), 935-941.

Leonard, W., Zhang, P., Ying, D., & Fang, Z. (2019). Hempseed in food industry: Nutritional value, health benefits, and industrial applications. *Comprehensive Reviews in Food Science and Food Safety, 19*, 282–308.

Li, J., Cha, R., Mou, K., Zhao, X., Long, K., Luo, H., ... & Jiang, X. (2018). Nanocellulose-Based Antibacterial Materials. *Advanced Healthcare Materials*, *7*(20), 1800334.

Li, X., Liu, Y., Jiang, Z., Li, R., Ren, X., & Huang, T. S. (2015). Synthesis of an N-halamine monomer and its application in antimicrobial cellulose via an electron beam irradiation process. *Cellulose*, *22*(6), 3609-3617.

Li, Y., Wang, Y., & Li, J. (2020). Antibacterial activity of polyvinyl alcohol (PVA)/ε-polylysine packaging films and the effect on longan fruit. *Food Science and Technology, 40*, 838-843.

Lin, K. H., Enomae, T., & Chang, F. C. (2019). Cellulose nanocrystal isolation from hardwood pulp using various hydrolysis conditions. *Molecules*, *24*(20), 3724.

Listyanda, R. F., Wildan, M. W., & Ilman, M. N. (2020). Preparation and characterization of cellulose nanocrystal extracted from ramie fibers by sulfuric acid hydrolysis. *Heliyon*, *6*(11), e05486.

Lizundia, E., Vilas, J. L., Sangroniz, A., & Etxeberria, A. (2017). Light and gas barrier properties of PLLA/metallic nanoparticles composite films. *European Polymer Journal*, *91*, 10-20.

Lu, D., Zhou, X., Xing, X., Wang, X., & Liu, Z. (2004). Quaternary ammonium salt (QAS) grafted cellulose fiber-preparation and anti-bacterial function. *Acta Polymerica Sinica*, (1), 107-113.

Luzi, F., Fortunati, E., Puglia, D., Lavorgna, M., Santulli, C., Kenny, J. M., & Torre, L. (2014). Optimized extraction of cellulose nanocrystals from pristine and carded hemp fibres. *Industrial Crops and Products*, *56*, 175-186.

Ma, H., Zhou, B., Li, H. S., Li, Y. Q., & Ou, S. Y. (2011). Green composite films composed of nanocrystalline cellulose and a cellulose matrix regenerated from functionalized ionic liquid solution. *Carbohydrate Polymers*, *84*(1), 383-389.

Mediavilla, V. & Steinemann, S. (1997). Essential oil of *Cannabis sativa* L. strains. Journal of the International Hemp Association. *Journal of the International Hemp Association, 4,* 80-82.

Moon, R.J., Martini, A., Nairn, J., Simonsen, J., & Youngblood, J. (2010). Cellulose nanomaterials review: structure, properties and nanocomposites. *The Royal Society of Chemistry, 40,* 3941-3994.

Muthulakshmi, L., Rajini, N., Nellaiah, H., Kathiresan, T., Jawaid, M., & Rajulu, A. V. (2017).

Preparation and properties of cellulose nanocomposite films with in situ generated copper nanoparticles using Terminalia catappa leaf extract. *International Journal of Biological Macromolecules*, *95*, 1064-1071.

Najjar, M. B., Kashtanov, D., & Chikindas, M. L. (2007). ε-Poly-l-lysine and nisin A act synergistically against Gram-positive food-borne pathogens *Bacillus cereus* and *Listeria monocytogenes*. *Letters in Applied Microbiology*, *45*(1), 13-18.

Nasri-Nasrabadi, B., Behzad, T., & Bagheri, R. (2014). Preparation and characterization of cellulose nanofiber reinforced thermoplastic starch composites. *Fibers and Polymers*, *15*(2), 347-354.

Oprea, M., & Panaitescu, D. M. (2020). Nanocellulose hybrids with metal oxides nanoparticles for biomedical applications. *Molecules*, *25*, 4045.

Oun, A. A., Shankar, S., & Rhim, J. W. (2020). Multifunctional nanocellulose/metal and metal oxide nanoparticle hybrid nanomaterials. *Critical Reviews in Food Science and Nutrition*, *60*, 435-460.

Pacaphol, K., & Aht-Ong, D. (2017). Preparation of hemp nanofibers from agricultural waste by mechanical defibrillation in water. *Journal of Cleaner Production*, *142*, 1283-1295.

Patiño-Masó, J., Serra-Parareda, F., Tarrés, Q., Mutjé, P., Espinach, F. X., & Delgado-Aguilar, M. (2019). TEMPO-oxidized cellulose nanofibers: a potential bio-based superabsorbent for diaper production. *Nanomaterials*, *9*(9), 1271.

Raghav, N., Sharma, M. R., & Kennedy, J. F. (2021). Nanocellulose: A mini-review on types and use in drug delivery systems. *Carbohydrate Polymer Technologies and Applications*, *2*, 100031.

Razali, N. A. M., Mohd Sohaimi, R., Othman, R. N. I. R., Abdullah, N., Demon, S. Z. N., Jasmani, L., ... & Halim, N. A. (2022). Comparative study on extraction of cellulose

fiber from rice straw waste from chemo-mechanical and pulping method. *Polymers*, *14*(3), 387.

Ren, L., He, G., Zhou, Y., Dai, J., Miao, W., Ouyang, C., ... & Chen, G. (2022). Hydrogel based on nanocellulose/polydopamine/gelatin are used for the treatment of MRSA infected wound with broad-spectrum antibacterial, antioxidant property and tissue suitability. *Biomaterials Science*, *10*, 3174-3187.

Restuccia, D., Spizzirri, U. G., Parisi, O. I., Cirillo, G., Curcio, M., Iemma, F., ... & Picci, N. (2010). New EU regulation aspects and global market of active and intelligent packaging for food industry applications. *Food Control*, *21*(11), 1425-1435.

Ribba, L., Garcia, N. L., D'Accorso, N., & Goyanes, S. (2017). Disadvantages of starch-based materials, feasible alternatives in order to overcome these limitations. In *Starch-based materials in food packaging* (pp. 37-76). Academic Press.

Rodrigues, B., Morais, T. P., Zaini, P. A., Campos, C. S., Almeida-Souza, H. O., Dandekar, A. M., ... & Goulart, L. R. (2020). Antimicrobial activity of Epsilon-Poly-l-lysine against phytopathogenic bacteria. *Scientific Reports*, *10*(1), 1-9.

Saini, S., Falco, Ç. Y., Belgacem, M. N., & Bras, J. (2016). Surface cationized cellulose nanofibrils for the production of contact active antimicrobial surfaces. *Carbohydrate Polymers*, *135*, 239-247.

Salgado, P. R., Di Giorgio, L., Musso, Y. S., & Mauri, A. N. (2021). Recent developments in smart food packaging focused on biobased and biodegradable polymers. *Frontiers in Sustainable Food Systems*, *5*, 125.

Salmieri, S., Islam, F., Khan, R. A., Hossain, F. M., Ibrahim, H. M., Miao, C., ... & Lacroix, M. (2014A). Antimicrobial nanocomposite films made of poly (lactic acid)–cellulose nanocrystals (PLA–CNC) in food applications—part B: effect of oregano essential oil

release on the inactivation of Listeria monocytogenes in mixed vegetables. *Cellulose*, *21*(6), 4271-4285.

Salmieri, S., Islam, F., Khan, R. A., Hossain, F. M., Ibrahim, H. M., Miao, C., ... & Lacroix, M. (2014B). Antimicrobial nanocomposite films made of poly (lactic acid)-cellulose nanocrystals (PLA-CNC) in food applications: part A—effect of nisin release on the inactivation of Listeria monocytogenes in ham. *Cellulose*, *21*(3), 1837-1850.

Sánchez-Gutiérrez, M., Bascón-Villegas, I., Espinosa, E., Carrasco, E., Pérez-Rodríguez, F., & Rodríguez, A. (2021). Cellulose nanofibers from olive tree pruning as food packaging additive of a biodegradable film. *Foods*, *10*(7), 1584.

Sánchez-López, E., Gomes, D., Esteruelas, G., Bonilla, L., Lopez-Machado, A. L., Galindo, R., Cano, A., Espina, M., Ettcheto, M., Camins, A., Silva, A. M., Durazzo, A., Santini, A., Garcia, M. L., & Souto, E. B. (2020). Metal-based nanoparticles as antimicrobial agents: an overview. *Nanomaterials*, *10*(2), 292.

Seddiqi, H., Oliaei, E., Honarkar, H., Jin, J., Geonzon, L. C., Bacabac, R. G., & Klein-Nulend, J. (2021). Cellulose and its derivatives: towards biomedical applications. *Cellulose*, *28*, 1893–1931.

Shahriari-Khalaji, M., Li, G., Liu, L., Sattar, M., Chen, L., Zhong, C., & Hong, F. F. (2022). A poly-l-lysine-bonded TEMPO-oxidized bacterial nanocellulose-based antibacterial dressing for infected wound treatment. *Carbohydrate Polymers*, *287*, 119266.

Sharma, C., & Bhardwaj, N. K. (2019). Bacterial nanocellulose: Present status, biomedical applications and future perspectives. *Materials Science and Engineering: C*, *104*, 109963.

Sharma, C., Bhardwaj, N. K., & Pathak, P. (2021). Static intermittent fed-batch production of bacterial nanocellulose from black tea and its modification using chitosan to develop antibacterial green packaging material. *Journal of Cleaner Production*, *279*, 123608.

Silvério, H. A., Flauzino Neto, W. P., & Pasquini, D. (2013). Effect of incorporating cellulose nanocrystals from corncob on the tensile, thermal and barrier properties of poly (vinyl alcohol) nanocomposites. *Journal of Nanomaterials*, *2013*.

Siripatrawan, U., & Harte, B. R. (2010). Physical properties and antioxidant activity of an active film from chitosan incorporated with green tea extract. *Food hydrocolloids*, *24*(8), 770-775.

Sivakanthan, S., Rajendran, S., Gamage, A., Madhujith, T., & Mani, S. (2020). Antioxidant and antimicrobial applications of biopolymers: A review. *Food Research International*, *136*, 109327.

Somvanshi, K. S., & Gope, P. C. (2021). Effect of ultrasonication and fiber treatment on mechanical and thermal properties of polyvinyl alcohol/cellulose fiber nano-biocomposite film. *Polymer Composites*, *42*(10), 5310-5322.

Song, K., Zhu, X., Zhu, W., & Li, X. (2019). Preparation and characterization of cellulose nanocrystal extracted from Calotropis procera biomass. *Bioresources and Bioprocessing*, *6*(1), 1-8.

Stanislawska, A. (2016). Bacterial nanocellulose as a microbiological derived nanomaterial. *Advances in Materials Science*, *16*, 45.

Stevulova, N., Cigasova, J., Estokova, A., Terpakova, E., Geffert, A., Kacik, F., ... & Holub, M. (2014). Properties characterization of chemically modified hemp hurds. *Materials*, *7*(12), 8131-8150.

Su, C., Huang, K., Li, H. H., Lu, Y. G., & Zheng, D. L. (2020). Antibacterial properties of functionalized gold nanoparticles and their application in oral biology. *Journal of Nanomaterials*, *2020*.

Sundaram, J., Pant, J., Goudie, M. J., Mani, S., & Handa, H. (2016). Antimicrobial and physicochemical characterization of biodegradable, nitric oxide-releasing

nanocellulose–chitosan packaging membranes. *Journal of Agricultural and Food Chemistry*, *64*(25), 5260-5266.

Suppakul, P. (2015). Active and intelligent packaging. *Polymers for Packaging Applications*, 393-428.

Syafiq, R., Sapuan, S. M., & Zuhri, M. R. M. (2021). Antimicrobial activity, physical, mechanical and barrier properties of sugar palm based nanocellulose/starch biocomposite films incorporated with cinnamon essential oil. *Journal of Materials Research and Technology*, *11*, 144-157.

Takahashi, M., Iyoda, K., Miyauchi, T., Ohkido, S., Tahashi, M., Wakita, K., ... & Hotta, K. (2009). Preparation and characterization of Eu: Ti codoped LiNbO 3 films prepared by the sol-gel method. *Journal of Applied Physics*, *106*(4), 044102.

Tan, Z., Shi, Y., Xing, B., Hou, Y., Cui, J., & Jia, S. (2019). The antimicrobial effects and mechanism of ε-poly-lysine against Staphylococcus aureus. *Bioresources and Bioprocessing*, *6*(1), 1-10.

Tarrés, Q., Boufi, S., Mutjé, P., & Delgado-Aguilar, M. (2017). Enzymatically hydrolyzed and TEMPO-oxidized cellulose nanofibers for the production of nanopapers: morphological, optical, thermal and mechanical properties. *Cellulose*, *24*(9), 3943-3954.

Tavakolian, M., Jafari, S.M., & van de Ven, T.G.M. (2020). A review on surface-functionalized cellulosic nanostructures as biocompatible antibacterial materials. *Nano-Micro Letters*, *12*, 73.

Thomas, P. S., Guerbois, J. P., Russell, G. F., & Briscoe, B. J. (2001). FTIR study of the thermal degradation of poly (vinyl alcohol). *Journal of Thermal Analysis and Calorimetry*, *64*(2), 501-508.

Tian, C., Yi, J., Wu, Y., Wu, Q., Qing, Y., & Wang, L. (2016). Preparation of highly charged

cellulose nanofibrils using high-pressure homogenization coupled with strong acid hydrolysis pretreatments. *Carbohydrate Polymers, 136,* 485-492.

Tischer, M., Pradel, G., Ohlsen, K., & Holzgrabe, U. (2012). Quaternary ammonium salts and their antimicrobial potential: targets or nonspecific interactions. *ChemMedChem, 7*(1), 22-31.

Tiseo, I. (2018). Global flow of plastic packaging waste 2015. Retrieved from https://www.statista.com/statistics/872408/plastic-packaging-waste-flow-worldwide/.

Trache, D., Hussin, M. H., Chuin, C. T. H., Sabar, S., Fazita, M. N., Taiwo, O. F., Hasan, T. M., & Haafiz, M. M. (2016). Microcrystalline cellulose: Isolation, characterization and bio-composites application—A review. *International Journal of Biological Macromolecules, 93,* 789-804.

Trache, D., Tarchoun, A. F., Derradji, M., Hamidon, T. S., Masruchin, N., Brosse, N., & Hussin, M. H. (2020). Nanocellulose: from fundamentals to advanced applications. *Frontiers in Chemistry, 8,* 392.

USDA. (2019). Industrial Hemp Production Trade and Regulation. Retrieved from https://apps.fas.usda.gov/newgainapi/api/report/downloadreportbyfilename?filename=Industrial%20Hemp%20Production%20Trade%20and%20Regulation_Ottawa_Canada_8-26-2019.pdf.

Van Rie, J., & Thielemans, W. (2017). Cellulose–gold nanoparticle hybrid materials. *Nanoscale, 9,* 8525-8554.

VanDolah, H. J., Bauer, B. A., & Mauck, K.F. (2019). Clinicians' Guide to Cannabidiol and Hemp Oils. *Mayo Clinic Proceedings, 94,* 1840-1851.

Vuerich, M., Ferfuia, C., Zuliani, F., Piani, B., Sepulcri, A., & Baldini, M., (2019). Yield and Quality of Essential Oils in Hemp Varieties in Different Environments. *Agronomy, 9,* Article 356.

Wahid, F., Wang, F. P., Xie, Y. Y., Chu, L. Q., Jia, S. R., Duan, Y. X., ... & Zhong, C. (2019). Reusable ternary PVA films containing bacterial cellulose fibers and ε-polylysine with improved mechanical and antibacterial properties. *Colloids and Surfaces B: Biointerfaces*, *183*, 110486.

Wang, Z., Qiao, X., & Sun, K. (2018). Rice straw cellulose nanofibrils reinforced poly (vinyl alcohol) composite films. *Carbohydrate Polymers*, *197*, 442-450.

Wei, L., Wu, R., Wang, C., & Wu, Z. (2017). Effects of ε-polylysine on Pseudomonas aeruginosa and Aspergillus fumigatus biofilm in vitro. *Medical Science Monitor: International Medical Journal of Experimental and Clinical Research*, *23*, 4225.

Wu, Y., Tang, Q., Yang, F., Xu, L., Wang, X., & Zhang, J. (2019). Mechanical and thermal properties of rice straw cellulose nanofibrils-enhanced polyvinyl alcohol films using freezing-and-thawing cycle method. *Cellulose*, *26*(5), 3193-3204.

Xie, Y. Y., Hu, X. H., Zhang, Y. W., Wahid, F., Chu, L. Q., Jia, S. R., & Zhong, C. (2020). Development and antibacterial activities of bacterial cellulose/graphene oxide-CuO nanocomposite films. *Carbohydrate Polymers*, *229*, 115456.

Yamada, H., Koike, N., Ehara, T., & Matsumoto, T. (2011). Measuring antimicrobial susceptibility of Pseudomonas aeruginosa using Poloxamer 407 gel. Journal of Infection and Chemotherapy, 17(2), 195-199.

Yi, T., Zhao, H., Mo, Q., Pan, D., Liu, Y., Huang, L., Xu, H., Hu, B., & Song, H. (2020). From cellulose to cellulose nanofibrils—a comprehensive review of the preparation and modification of cellulose nanofibrils. *Materials, 13,* Article 5062.

Yildirim, S. (2011). Active packaging for food biopreservation. In *Protective cultures, antimicrobial metabolites and bacteriophages for food and beverage biopreservation* (pp. 460-489). Woodhead Publishing.

Yildirim, S., & Röcker, B. (2018). Active packaging. In *Nanomaterials for Food Packaging* (pp. 173-202). Elsevier.

Yildirim, S., Röcker, B., Pettersen, M.K., Nilsen-Nygaard, J., Ayhan, Z., Rutkaite, R., Radusin, T., Suminska, P., Marcos, B., & Coma, V. (2018). Active Packaging Applications for Food. *Comprehensive Reviews in Food Science and Food Safety, 17,* 165-199.

You, X., Einson, J. E., Lopez-Pena, C. L., Song, M., Xiao, H., McClements, D. J., & Sela, D. A. (2017). Food-grade cationic antimicrobial ε-polylysine transiently alters the gut microbial community and predicted metagenome function in CD-1 mice. *NPJ science of Food*, *1*(1), 1-10.

Yu, Z., Alsammarraie, F. K., Nayigiziki, F. X., Wang, W., Vardhanabhuti, B., Mustapha, A., & Lin, M. (2017). Effect and mechanism of cellulose nanofibrils on the active functions of biopolymer-based nanocomposite films. *Food Research International*, *99*, 166-172.

Yu, Z., Dhital, R., Wang, W., Sun, L., Zeng, W., Mustapha, A., & Lin, M. (2019a). Development of multifunctional nanocomposites containing cellulose nanofibrils and soy proteins as food packaging materials. *Food Packaging and Shelf Life*, *21*, 100366.

Yu, Z., Rao, G., Wei, Y., Yu, J., Wu, S., & Fang, Y. (2019b). Preparation, characterization, and antibacterial properties of biofilms comprising chitosan and ε-polylysine. *International Journal of Biological Macromolecules*, *141*, 545-552.

Zhang, X., Shi, C., Liu, Z., Pan, F., Meng, R., Bu, X., ... & Yu, L. (2018). Antibacterial activity and mode of action of ε-polylysine against Escherichia coli O157: H7. *Journal of Medical Microbiology*, *67*(6), 838-845.

Zhang, Y., Liu, Y., Li, R., Ren, X., & Huang, T. S. (2019B). Preparation and characterization of antimicrobial films based on nanocrystalline cellulose. *Journal of Applied Polymer Science*, *136*(8), 47101.

Zhang, Y., Yin, M., Lin, X., Ren, X., Huang, T. S., & Kim, I. S. (2019A). Functional nanocomposite aerogels based on nanocrystalline cellulose for selective oil/water separation and antibacterial applications. *Chemical Engineering Journal, 371*, 306-313.

Zhu, H., Jia, S., Yang, H., Tang, W., Jia, Y., & Tan, Z. (2010). Characterization of bacteriostatic sausage casing: A composite of bacterial cellulose embedded with ε-polylysine. *Food Science and Biotechnology, 19*(6), 1479-1484.